

New measurements of lightning electric fields in Florida: Waveform characteristics, interaction with the ionosphere, and peak current estimates

Michael A. Haddad,^{1,2} Vladimir A. Rakov,¹ and Steven A. Cummer³

Received 18 November 2011; revised 29 March 2012; accepted 31 March 2012; published 16 May 2012.

[1] We analyzed wideband electric field waveforms of 265 first and 349 subsequent return strokes in negative natural lightning. The distances ranged from 10 to 330 km. Evolution of first- and subsequent-stroke field waveforms as a function of distance is examined. Statistics on the following field waveform parameters are given: initial electric field peak, opposite-polarity overshoot, ratio of the initial electric field peak to the opposite polarity overshoot, zero-to-peak risetime, initial half-cycle duration, and opposite polarity overshoot duration. The overwhelming majority of both first and subsequent return-stroke field waveforms at 50 to 330 km exhibit an opposite polarity overshoot. At distances greater than 100 km, electric field waveforms, recorded under primarily daytime conditions, tend to be oscillatory. Using finite difference time domain modeling, we interpreted the initial positive half-cycle and the opposite-polarity overshoot as the ground wave and the second positive half-cycle as the one-hop ionospheric reflection. The observed difference in arrival times of these two waves for subsequent strokes is considerably smaller than for first strokes, suggesting that the first-stroke electromagnetic field caused a descent of the ionospheric D-layer. We speculate that there may be cumulative effect of multiple strokes in lowering the ionospheric reflection height. Return-stroke peak currents estimated from the empirical formula, $I = 1.5 - 0.037DE$ (where I is considered negative and in kA, E is the electric field peak considered positive and in V/m, and D is distance in km), are compared to those reported by the NLDN.

Citation: Haddad, M. A., V. A. Rakov, and S. A. Cummer (2012), New measurements of lightning electric fields in Florida: Waveform characteristics, interaction with the ionosphere, and peak current estimates, *J. Geophys. Res.*, 117, D10101, doi:10.1029/2011JD017196.

1. Introduction

[2] *Lin et al.* [1979] examined in detail wideband electric field waveforms (also magnetic field waveforms, not considered here) produced by both first and subsequent return strokes in Florida negative lightning flashes at distances of 1 to 200 km. Their typical waveforms, often used as a benchmark for testing validity of various lightning return-stroke models, are reproduced, for the distance range of 10 to 200 km, in Figure 1. The characteristic features of these waveforms include (1) a sharp initial peak that varies

approximately as the inverse distance, (2) a slow ramp following the initial peak and lasting in excess of 100 μ s for electric fields measured within a few tens of kilometers, and (3) a zero crossing within tens of microseconds of the initial peak at 50 to 200 km. Similar studies were performed in Sweden and Sri Lanka [*Cooray and Lundquist*, 1982, 1985]. Also, *Taylor* [1963] examined in detail electric field waveforms of 47 first return strokes in the 100 to 500 km range in Oklahoma.

[3] In order to verify the characteristic features (in particular the zero-crossing time) of distant electric field waveforms identified by *Lin et al.* [1979], *Pavlick et al.* [2002] acquired a new, larger data set for Florida negative lightning, which included electric field waveforms of 178 first return strokes. The data were obtained at Camp Blanding, Florida, in 1998 and 1999. The distances, reported by the U.S. National Lightning Detection Network (NLDN), ranged from 50 to 250 km. Evolution of typical electric field waveforms for first return strokes as a function of distance was examined, and statistics on electric field waveform parameters were given. They found that about 4% of the 178 waveforms did not exhibit a pronounced opposite-polarity overshoot within 400 μ s of the initial peak, although at distances greater than 50 km all the

¹Department of Electrical and Computer Engineering, University of Florida, Gainesville, Florida, USA.

²Now at Department of Electrical Engineering, University of California, Los Angeles, California, USA.

³Electrical and Computer Engineering Department, Duke University, Durham, North Carolina, USA.

Corresponding author: V. A. Rakov, Department of Electrical and Computer Engineering, University of Florida, 553 Engineering Bldg. 33, Gainesville, FL 32611, USA. (rakov@ece.ufl.edu)

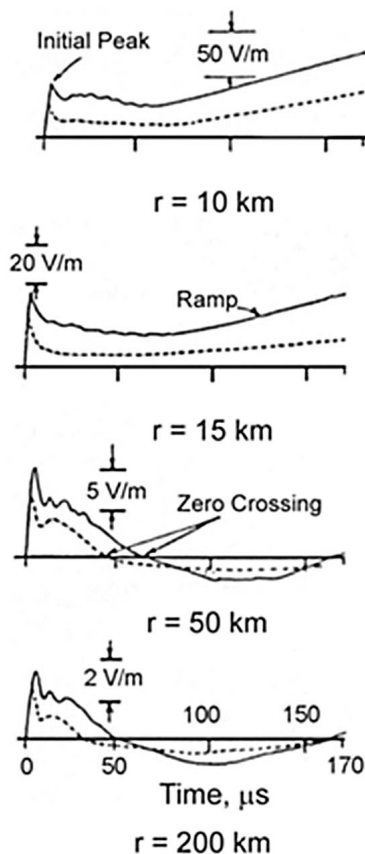


Figure 1. Typical vertical electric field intensity waveforms for first (solid line) and subsequent (dashed line) return strokes at distances of 10, 15, 50, and 200 km. Adapted from *Lin et al.* [1979].

waveforms are expected [*Lin et al.*, 1979] to do so. Pavlick et al. also estimated return-stroke peak currents from measured electric fields and NLDN-reported distances using the empirical formula of *Rakov et al.* [1992], $I = 1.5 - 0.037DE$, where I is the return-stroke peak current, considered negative and in kA, E is the electric field peak considered positive and in V/m, and D is distance in km. This empirical formula is based on triggered-lightning data of *Willett et al.* [1989] and, strictly speaking, is applicable only to subsequent strokes. Nevertheless, Pavlick et al. applied the formula to their first strokes and compared the resultant peak currents to corresponding peak currents reported by the NLDN. The latter were on average about 10% lower than the values predicted by the empirical formula.

[4] The present study can be viewed as an extension of *Pavlick et al.*'s [2002] work to additionally examine subsequent strokes, not included by Pavlick et al. in their analysis. Further, we consider a slightly larger range of distances, from 10 to 330 km, and use a slightly longer time scale (600 μ s versus 500 μ s in Pavlick et al.'s study) to display our electric field waveforms. Finally, our instrumentation decay time constant, 10 ms, was considerably longer than that of Pavlick et al., less than 800 μ s, which allowed us to avoid waveform distortion likely present in their study. We also broadened the scope of the previous study by examining ionospheric reflection signatures. The field waveform characteristics

examined here are needed for testing the validity of various lightning return-stroke models [e.g., *Rakov and Uman*, 1998].

[5] It is worth noting that the NLDN has recently undergone an upgrade (completed in 2004). Prior to the upgrade, the NLDN consisted of 106 sensors: 63 LPATS III sensors, which provided only time-of-arrival information, and 43 IMPACT sensors, which provided both time-of-arrival and azimuth information. During the upgrade, all sensors in the NLDN were replaced with IMPACT-ESP sensors having improved analog front-end circuitry, higher-speed processor, and configurable waveform criteria. The total number of sensors is currently 114. A detailed description of the upgrade is given by *Cummins and Murphy* [2009]. The NLDN field-to-current conversion procedure was modified on July 1, 2004 by changing the field propagation model from power law to exponential. The latter apparently served to improve the accuracy of NLDN current estimates [*Nag et al.*, 2011a], at least for subsequent strokes.

2. Instrumentation and Data

[6] Data examined in this paper were acquired on five days during May and June of 2009 at the Lightning Observatory in Gainesville (LOG), located on the roof of the five-story New Engineering Building at the University of Florida campus.

[7] An elevated flat-plate antenna with its sensing plate at a height of 1.6 m above roof level was used to record the electric field waveforms. The antenna was connected, via appropriate electronics and a fiber optic link, to an 8-bit LeCroy WavePro 7100A digitizing oscilloscope sampling at 100 MHz. The record length was 500 ms including pre-trigger time of 100 ms. The system had a useful (3-dB) frequency bandwidth of 16 Hz to at least 10 MHz. The instrumentation decay time constant was 10 ms, much longer than the duration of field waveforms (500 μ s) examined in this paper. More details on the field measuring system at LOG can be found in *Nag* [2010].

[8] No voltage amplification was used for recording relatively close (10–40 km) events, just an integrator and a high-input-impedance, unity-gain amplifier were used. Most of the intermediate-range (40–150 km) and distant-range (beyond 150 km) events were recorded with amplification of 3 and 8.8, respectively. An oscilloscope trigger level of 250 mV was used when no amplification was applied, and for events recorded with amplification the trigger level was 300 mV. The trigger thresholds (selected empirically) were relatively high to minimize triggering on cloud-discharge pulses. In spite of higher gains used for recording signals from more distant sources, our data set is biased toward more intense sources, as further discussed in section 4.2.1.

[9] Recorded electric field waveforms were matched to GPS timestamps created upon a signal exceeding the oscilloscope threshold level. LOG and NLDN time stamps matching with a tolerance of 100 μ s were used to identify NLDN data for first strokes recorded at LOG. Subsequent strokes were identified in the NLDN database using inter-stroke intervals. For each electric field waveform included in the analysis, we obtained from the NLDN database the latitude, longitude, polarity, and estimated return-stroke peak current, I_{NLDN} .

[10] A lightning event was included in the analysis only if it was recorded by the NLDN and its electric field waveform had a signal-to-noise ratio exceeding approximately 3. The latter requirement allowed the features such as peak electric field and zero-to-peak risetime to be reliably resolved. Lightning cloud-to-ground flashes that had been preceded by significant in-cloud activity (other than the preliminary breakdown process) were not included in this study.

[11] Some strokes observed at LOG were not reported by the NLDN. For 111 first strokes that occurred during a two-hour period of the 6/5/2009 storm and were recorded at LOG, 20 were missed by the NLDN. The resultant first stroke detection efficiency is $20/111 = 0.82$. For the NLDN-located strokes from this storm, distances ranged from 120 to 327 km with the mean value being 220 km. We used this mean distance (which is not far from the mean distance of 250 km for 16 out of the 20 NLDN-missed strokes reported by the World Wide Lightning Location Network [Rodger *et al.*, 2006; Hutchins *et al.*, 2012]), LOG-measured field peaks, and the empirical formula of Rakov *et al.* [1992] to estimate current peaks for the 20 first strokes not reported by the NLDN. The peak currents were considerably larger than average, ranging from 86 to 273 kA with a mean value of 138 kA. This finding is important, because larger strokes are usually a greater threat to various objects and systems. The majority of the NLDN-missed events (14 out of 20) were single strokes within 500-ms records, 17 exhibited step pulses, and 9 were preceded by preliminary-breakdown pulse trains. We speculate that for at least some of these events the non-reporting by the NLDN could be attributed to pronounced step pulses prior to return-stroke waveforms. Such possibility was discussed by Cummins [2000] for April, May, and August storms in North America and by Honma [2010] and Cummins *et al.* [2010, 2011] for the case of winter storms in Japan.

[12] The detection efficiency of the NLDN for subsequent strokes was lower (a quantitative estimate is not available at this time), as expected. This can be attributed to the lower peak currents and, as a result, the less pronounced electric field signatures observed for subsequent strokes. The lower detection efficiency for lower intensity strokes in triggered lightning was documented by Jerauld *et al.* [2005] and Nag *et al.* [2011a].

[13] The data set examined here includes 265 first and 349 subsequent return strokes from Florida negative flashes that occurred at distances ranging from 10 to 330 km from the field-measuring station (LOG). We did not make any distinction between subsequent strokes following a previously formed channel and those creating a new termination on ground. From the point of view of electric field wave-shape parameters, these are apparently the largest sample sizes as of today [see Rakov and Uman, 2003, Table 4.6]. Also, the longer time scale (600 μ s, with the return stroke onset at 100 μ s after the beginning of the displayed record) that we employed for our field waveforms allowed us to identify features not recognized in previous studies in which less than 200 μ s from the return stroke onset were examined [e.g., Lin *et al.*, 1979]. Specifically, our waveforms recorded (primarily under daytime conditions) at distances greater than 100 km or so exhibit ionospheric reflections, which can be used to study lightning interaction with the ionosphere [e.g., Inan *et al.*, 2010].

[14] The atmospheric electricity sign convention (a downward-directed electric field change vector is considered positive) is used throughout this paper.

3. Methodology

[15] The latitude and longitude reported by the NLDN for each stroke were used to calculate the distance (in km) from the field measuring point (LOG), 29.65°N 82.35°W, using the following formula [Pavlick *et al.*, 2002]:

$$D = 2R_e \sin^{-1} \sqrt{\sin^2 \frac{(\theta_o - \theta_e)}{2} + \cos \theta_o \cos \theta_e \sin^2 \frac{(\phi_o - \phi_e)}{2}} \quad (1)$$

where $R_e = 6367$ km is the radius of the Earth (assumed to be a perfect sphere), θ_o is the latitude of the LOG in degrees, θ_e is the latitude of the lightning event in degrees, ϕ_o is the longitude of the LOG in degrees, ϕ_e is the longitude of the lightning event in degrees.

[16] The electric field was calculated from the digitizer-recorded voltage, V_d , as:

$$E = \frac{V_d C}{G A \epsilon_o} \quad (2)$$

where C is the integrator capacitance, 10.4 nF, A is the area of the flat-plate antenna, 0.2 m², G is the overall gain of the system, and ϵ_o is the electric permittivity of free space. The overall gain of the system was found as the product of the experimentally found field enhancement due to elevation of antenna sensing plate above the roof of the building, $G_a = 11$, field enhancement due to placing the antenna on the five-story building, $G_b = 1.4$ [Baba and Rakov, 2007], and a fiber optic link gain of 1.4, so that $G = 21.6$. A detailed description of the different components of G is found in Nag [2010].

[17] The initial electric field peak was calculated as:

$$E_p = E_{\max} - E_{\text{ref}} \quad (3)$$

where E_{\max} is the maximum electric field value measured with respect to the zero level, and E_{ref} is the reference (background) electric field level tens of microseconds prior to the lightning return stroke waveform with respect to the zero level. E_{ref} was negligible for events occurring beyond 50 km or so. The opposite polarity overshoot was calculated as:

$$E_{os} = E_{\text{ref}} - E_{\min} \quad (4)$$

where E_{\min} is the first negative (atmospheric electricity sign convention) minimum electric field value within 400 μ s after the initial peak, measured with respect to the zero level. This definition of opposite polarity overshoot is the same as that employed by Pavlick *et al.* [2002].

[18] The initial half-cycle duration (first zero-crossing time), T_1 , is measured between the initial deflection from the reference level and the first reference level crossing after the initial peak. The opposite polarity overshoot duration, T_2 , is measured between the end of T_1 and the first reference level crossing after the opposite polarity overshoot. When ringing occurs around the reference level, an average is taken to determine the reference level crossing point. The zero-to-peak risetime, T_R , is measured between the initial deflection from

Table 1. Number of Strokes in Different Distance Ranges^a

Distance Range (km)	First Strokes	Subsequent Strokes	Total
0–50	102 (20%)	152 (11%)	257 (15%)
50–100	54 (89%)	68 (72%)	122 (79%)
100–150	22 (100%)	28 (93%)	50 (96%)
150–200	29 (100%)	37 (97%)	66 (98%)
200–250	34 (97%)	47 (98%)	81 (99%)
250–300	17 (100%)	11 (100%)	28 (100%)
300–350	7 (100%)	6 (100%)	13 (100%)
0–350	265 (67%)	349 (54%)	614 (60%)
50–350	163 (96%)	197 (88%)	360 (92%)

^aThe percentages of strokes exhibiting an opposite polarity overshoot are listed in parentheses.

the reference level to the field peak. Measurements of all the waveform parameters are illustrated in Figure 4.

[19] Following Pavlick *et al.* [2002], we will estimate lightning peak currents, I , from measured fields, E , and NLDN-reported distances, D , using the following regression equation derived by Rakov *et al.* [1992]:

$$I = 1.5 - 0.037 * D * E \quad (5)$$

where I is in kA and taken as negative, E is positive and in V/m, and D is the distance in km. The data used in deriving equation (5) were acquired, for 28 triggered-lightning strokes, by Willett *et al.* [1989]. Scaling of the field peaks from 5.16 km (distance at which the triggered-lightning fields were measured) to an arbitrary distance D was done assuming that the field varies inversely with distance, as expected for the radiation field component. As noted in section 1, the formula is expected to apply to negative subsequent strokes, but is employed here, following Pavlick *et al.* [2002], for negative first strokes as well.

[20] The percent difference between the NLDN-reported peak current, I_{NLDN} , and peak current estimated from (5) is given by:

$$\Delta I, \% = \frac{|I_{NLDN}| - |I|}{|I|} * 100\% \quad (6)$$

According to equation (6), a negative ΔI value means underestimation of peak current by the NLDN.

[21] The peak current (in kA) reported by the NLDN is calculated using the following equation:

$$I_{NLDN} = 0.185 * Mean(RNSS) \quad (\text{kA}) \quad (7)$$

where $Mean(RNSS)$ is the arithmetic mean of range-normalized (to 100 km) magnetic field signal strengths, in so-called LLP units, from all sensors allowed by the central analyzer to participate in the peak current estimate. Normalization to 100 km involves a field propagation model, designed to compensate for field attenuation due to its propagation over lossy ground. A detailed description of the RNSS calculation is given by Nag *et al.* [2011b].

4. Analysis and Discussion

[22] Numbers of first and subsequent strokes in different distance ranges are given in Table 1. The percentages of strokes exhibiting an opposite polarity overshoot (OPO) are

listed in the parentheses. The overwhelming majority of both first and subsequent return stroke field waveforms at 50 to 350 km (96 and 88%, respectively) exhibit OPOs. The percentage of first strokes showing OPO is the same as in Pavlick *et al.*'s [2002] work. Subsequent stroke signatures at 50 to 100 km are appreciably less likely (72% versus 89%) to be bipolar than their first-stroke counterparts. This is apparently in contrast with Lin *et al.*'s [1979] results (see Figure 1), according to which both first and subsequent stroke signatures at 50 km are expected to be bipolar. Shoory *et al.* [2009], based on modeling, suggested that the first zero-crossing time in far-field waveforms is influenced by the duration of the return-stroke current waveform, the current attenuation along the channel, and the return-stroke speed. Other influencing factors include the variation of return-stroke speed along the channel [e.g., Thottappillil *et al.*, 1991] and channel geometry [Cooray *et al.*, 2008]. We plan to examine all these and other factors in view of our new electric field observations in a future paper. For both first and subsequent strokes combined, 92% of the 360 events at distances beyond 50 km exhibited OPOs. On the other hand, 54 out of 56 strokes within 30 km and 20 out of 46 strokes in the 30–50 km range show no OPO. The observed lack of OPOs at relatively close distances is expected and is primarily due to the influence of the electrostatic ramp (see Figure 1).

4.1. Evolution of Electric Field Waveforms With Distance

[23] Typical waveforms for first strokes as a function of distance are shown in Figure 2. The waveforms represent distance ranges of 0–50 km, 50–100 km, 100–150 km, 150–200 km, 200–250 km, 250–300 km, and 300–350 km. Similarly, typical waveforms for subsequent strokes are shown in Figure 3.

[24] As expected, a significant electrostatic ramp is seen in both first and subsequent stroke waveforms at distances less than 50 km (in the 0–50 km range). For all other distance ranges, the electric field usually changes polarity three times (if the fine structure is ignored), so that the waveforms appear oscillatory, showing two cycles within 500 μs , with the corresponding frequency being about 4–5 kHz. This oscillatory behavior is particularly pronounced at distances exceeding 100 km. The magnitudes of the first negative and second positive half-cycles, relative to the initial positive half-cycle, increase with increasing distance. Further, they are appreciably smaller for subsequent strokes than for first strokes (this will be quantified for the first negative half-cycle below).

4.2. Statistics on Waveform Parameters

[25] Definitions of electric field waveform parameters are illustrated in Figure 4. Statistical characteristics (Arithmetic Mean, Geometric Mean, and Standard Deviation of the Logarithm (base 10) of Parameter) of the waveform parameters, as well as of I_{NLDN} , I , and ΔI , for first and subsequent strokes are summarized in Tables 2a, 2b and 2c and Tables 3a, 3b and 3c, respectively. The characteristics are given for the same distance ranges as in Figures 2 and 3 and additionally for all data combined (10–330 km) and for the 50–330 km range, where the electric field waveforms are expected [Lin *et al.*, 1979] to be dominated by the radiation

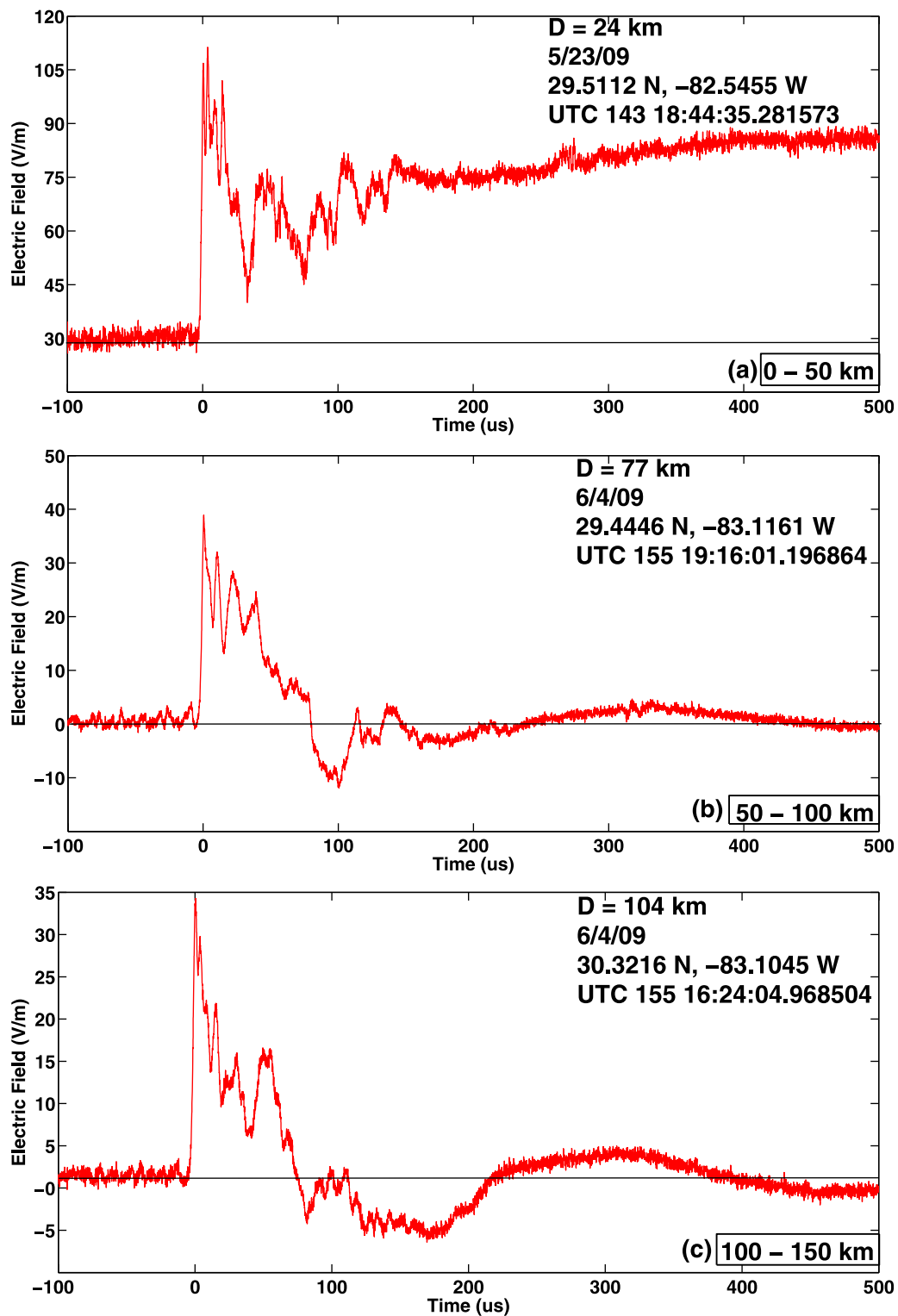


Figure 2. Typical electric field waveforms for first return strokes as a function of distance: (a) 0–50 km, (b) 50–100 km, (c) 100–150 km, (d) 150–200 km, (e) 200–250 km, (f) 250–300 km, and (g) 300–350 km.

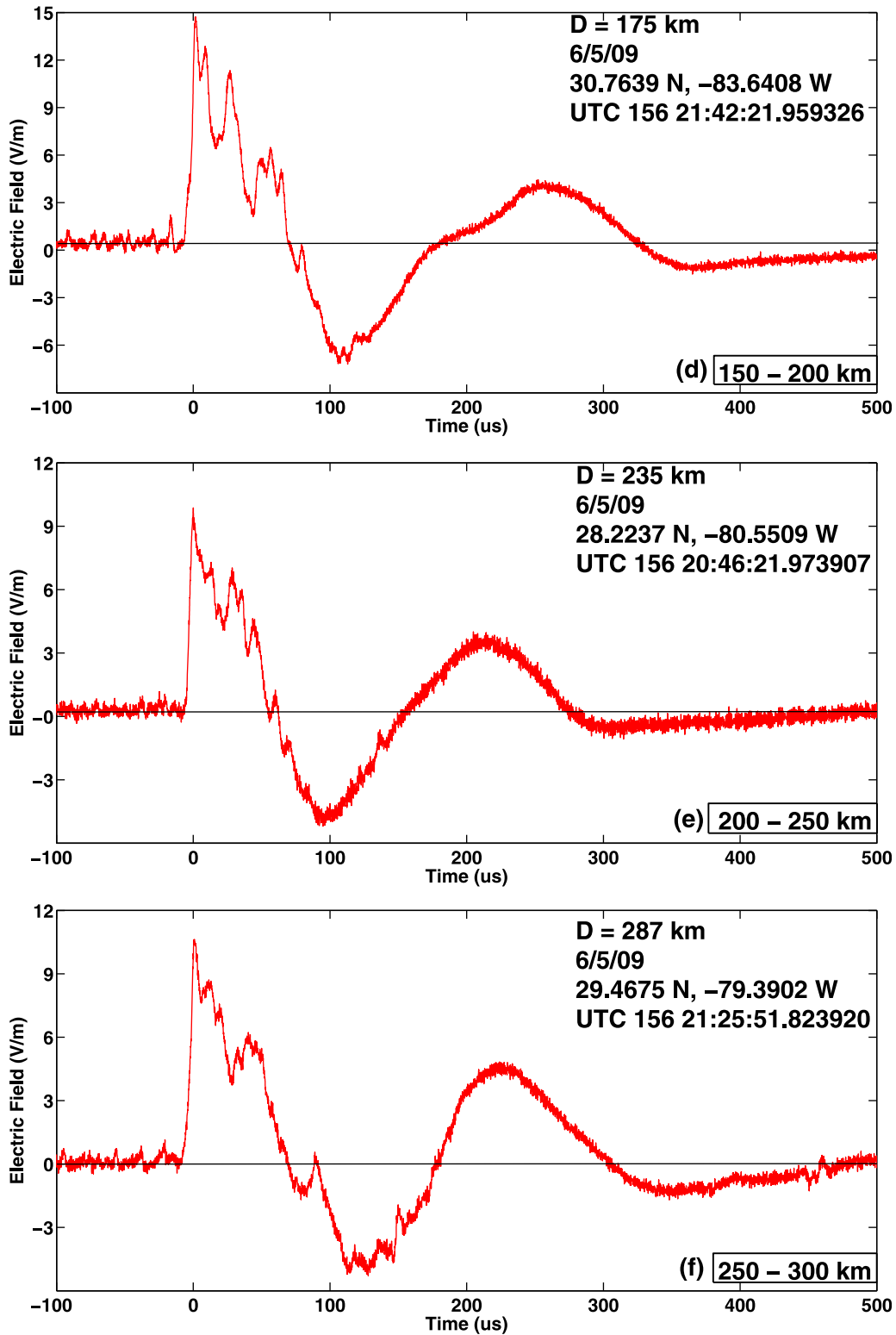


Figure 2. (continued)

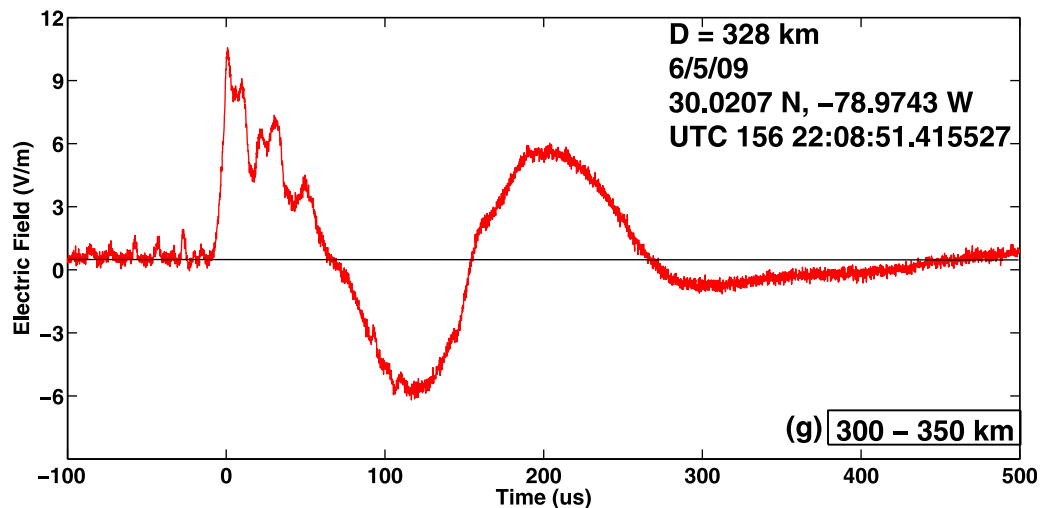


Figure 2. (continued)

field component. Histograms of all the waveform parameters (regardless of distance) for first and subsequent strokes are shown in Figures 5 and 6, respectively.

4.2.1. Initial Electric Field Peak

[26] The geometric mean (GM) initial electric field peaks normalized to 100 km in our data set, 25 V/m and 9.7 V/m for all first and all subsequent strokes, respectively, are considerably larger than their typical values [e.g., *Rakov and Uman*, 2003, Table 4.6] of about 6 V/m for first strokes and 3 V/m for subsequent ones. This is because we employed a triggered field measuring system with relatively high thresholds (see section 1) to minimize triggering on cloud discharge pulses. Since the bias toward larger events is evident for both first and subsequent strokes, there should be positive correlation between their distance-normalized initial field peaks (and, by inference, peak currents). We assume that the field waveform characteristics that are examined in this paper are not materially influenced by our bias toward larger-amplitude events. As of today, there are no observations that would make us believe otherwise; and this is a generally accepted assumption in lightning modeling [e.g., *Rakov and Uman*, 2003, chap. 12, and references therein]. Interestingly, when we exclude all strokes at distances less than 50 km, the GM (also arithmetic mean, AM) initial electric field peak normalized to 100 km somewhat increases for first strokes, but remains the same (practically the same for AM) for subsequent ones. This is an indication of stronger trigger-related bias for first strokes (the measuring system essentially always triggered on first strokes), even overwhelming the expected opposite trend for the 10 to 50 km range due to possible contribution to the field peak from the electrostatic and induction components.

4.2.2. Zero-to-Peak Risetime

[27] The arithmetic mean (AM) and geometric mean (GM) zero-to-peak risetimes for first strokes are 7.7 and 7.1 μs (8.5 and 7.9 μs , if we exclude the events at distances less than 50 km), respectively. Their counterparts for subsequent strokes are smaller, 5.0 and 4.4 μs (5.1 and 4.6 μs , if we exclude the events at distances less than 50 km), as expected. Our risetimes are larger than those reported by *Lin et al.* [1979], *Cooray and Lundquist* [1982], and *Master et al.* [1984]. The AM zero-to-

peak risetime reported by *Pavlick et al.* [2002] for first strokes at distances in the 50 to 250 km range is 8.3 μs , similar to our 8.5 μs . There is no clear distance dependence of the zero-to-peak risetime for either first or subsequent strokes.

4.2.3. Initial Half-Cycle Duration

[28] The arithmetic mean (AM) and geometric mean (GM) initial half-cycle durations (first zero-crossing times) for first strokes are 89 and 86 μs , respectively. For comparison, AM values of this parameter reported by *Taylor* [1963], *Lin et al.* [1979], and *Pavlick et al.* [2002] are 53, 54, and 50 μs , respectively. We believe that the latter three values are underestimates, due to insufficiently long instrumental decay time constant (159 μs , which corresponds to the 1-kHz lower frequency response, in Taylor's study and 774 μs or less in that of Pavlick et al.) or the use of 2.5- μs delay lines, which could be insufficient for determining the actual zero-field level in *Lin et al.*'s work. Our records (10-ms instrumental decay time constant and 100-ms pretrigger) are free of those deficiencies. Additionally, *Lin et al.* [1979] included subsequent strokes with leader durations of a few milliseconds or more (possibly creating new terminations on ground) in the first-stroke category, which could bias the true-first-stroke statistics. AM zero-crossing times reported by *Cooray and Lundquist* [1985] from their measurements in Sweden and Sri Lanka are 49 and 89 μs (instrumental decay time constant was reportedly 100 ms), the latter value being equal to our estimate in Florida.

[29] For subsequent strokes, our AM and GM initial half-cycle durations are 68 and 62 μs (69 and 62 μs , if events at distances less than 50 km are excluded), respectively. The corresponding AM values previously reported for Florida, Sweden, and Sri Lanka are 39, 42, and 36 μs [*Lin et al.*, 1979; *Cooray and Lundquist*, 1985]. Our values are appreciably longer than those based on earlier observations.

4.2.4. Opposite-Polarity Overshoot Duration

[30] The AM and GM opposite polarity overshoot (OPO) durations, T_2 , for first strokes are larger than the AM and GM initial half-cycle durations, 107 and 91 μs (116 and 111 μs , if strokes at distances less than 50 km are excluded) versus 89 and 86 μs for both cases. The AM and GM OPO duration values in *Pavlick et al.*'s [2002] study are 90 and 72 μs ,

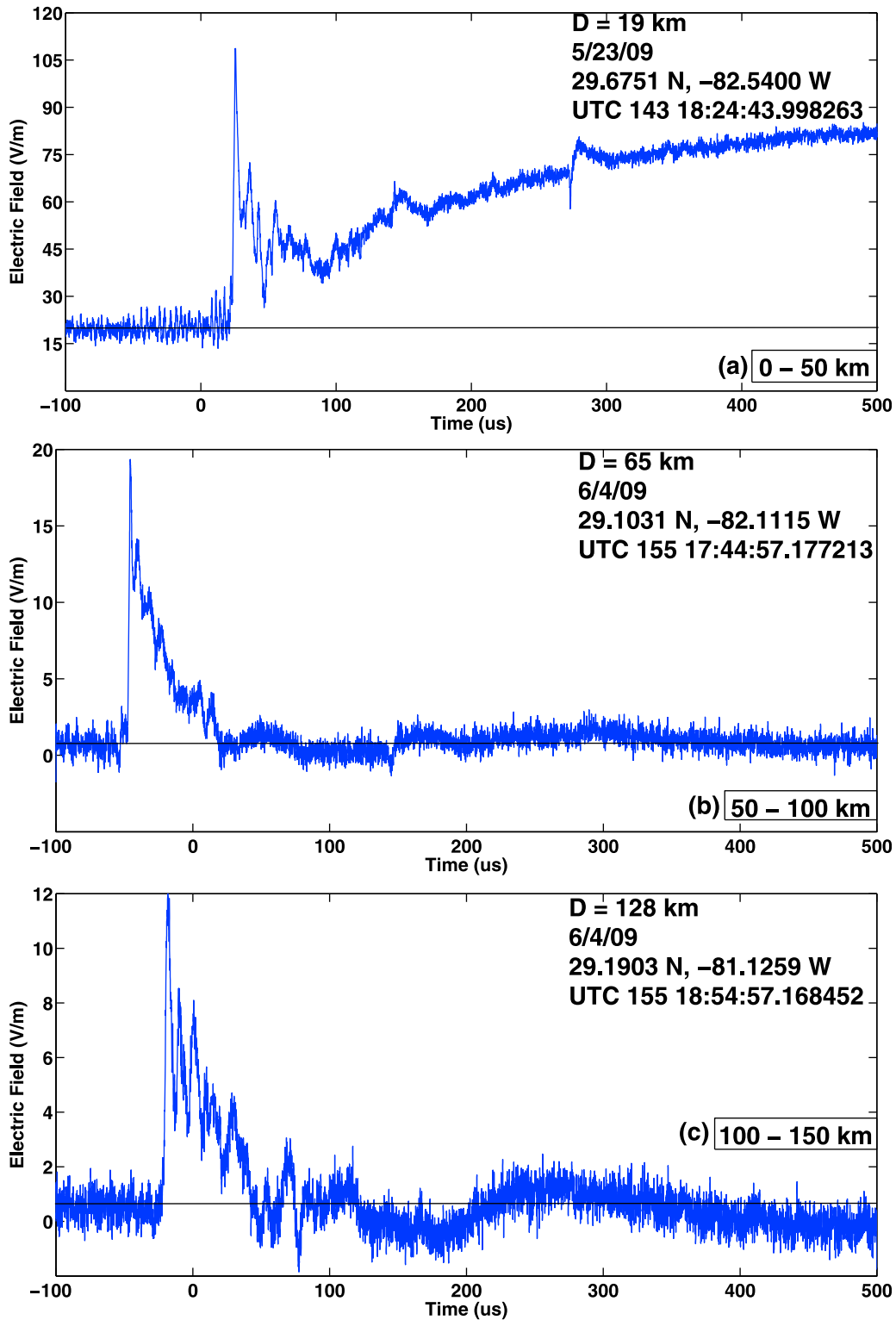


Figure 3. Typical electric field waveforms for subsequent return strokes as a function of distance: (a) 0–50 km, (b) 50–100 km, (c) 100–150 km, (d) 150–200 km, (e) 200–250 km, (f) 250–300 km, and (g) 300–350 km.

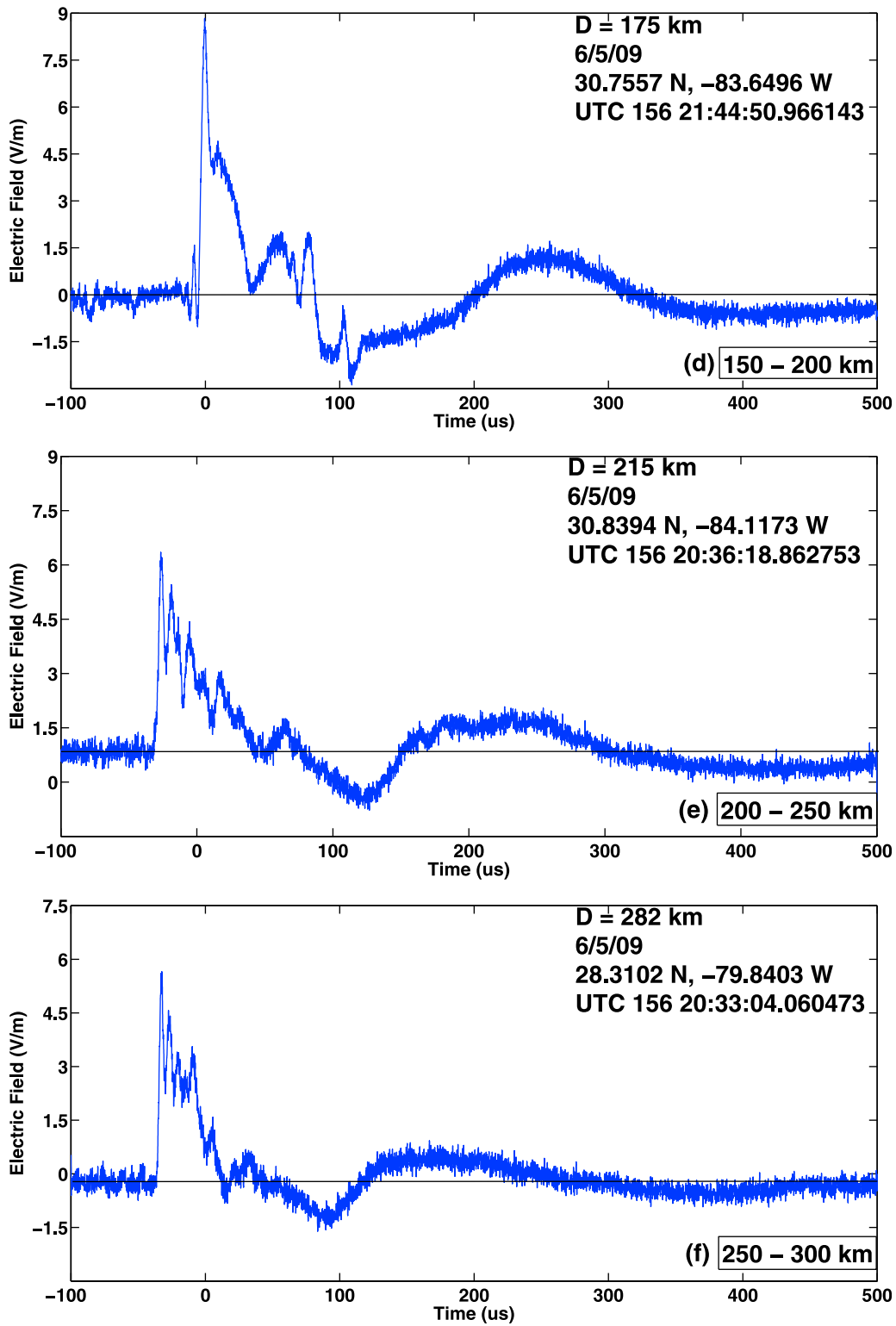


Figure 3. (continued)

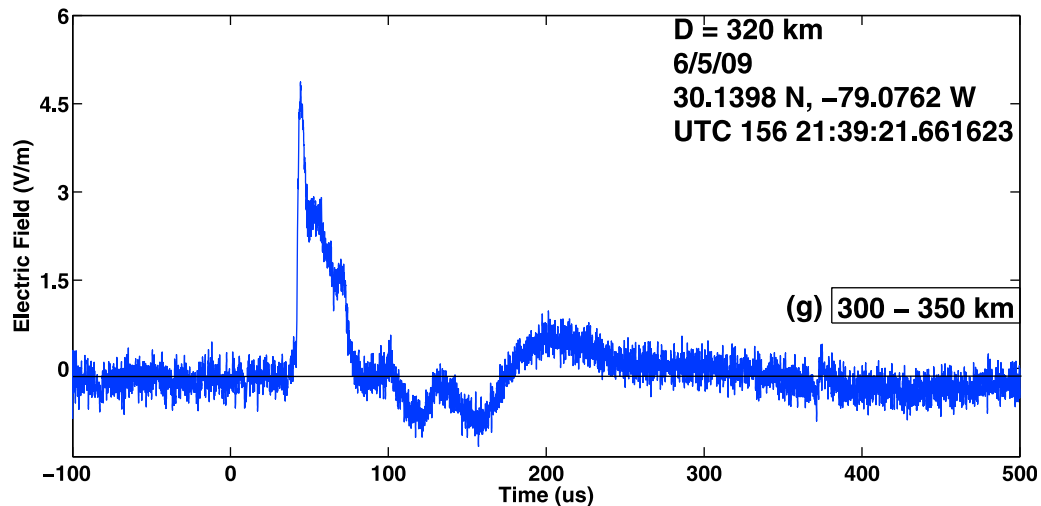


Figure 3. (continued)

respectively, and, similar to first zero-crossing times are probably influenced by the instrumental decay.

[31] For subsequent strokes, the AM and GM OPO durations in our study are 80 and 58 μs (86 and 65 μs , if strokes at distances less than 50 km are excluded), respectively, with the GM of 58 μs being slightly smaller than the corresponding GM first zero-crossing time, T_1 , of 62 μs . We are not aware of similar measurements of OPO duration (other than the Pavlick et al.'s study discussed above).

4.2.5. Ratio of Initial Electric Field Peak to Opposite Polarity Overshoot

[32] The AM and GM ratios of initial electric field peak (IEFP) to OPO for our first strokes are 4.3 and 3.5 (3.5 and 3.1, if strokes at distances less than 50 km are excluded), respectively. The corresponding values in Pavlick et al.'s [2002] study are 5.4 and 5.2 for the 50 to 250 km range, and Taylor [1963] reported the AM value of about 3.3 for the 100 to 500 km range. The ratio appears to be strongly influenced by the distance: the AM value ranges from 9.8 at distances less than 50 km (definitely affected by the electrostatic

and induction components) to 4.4 in the 50–100 km range to 2 to 3 in the 250–350 km range. Our AM value for the 50–350 km range is 3.5, close to that of Taylor [1963].

[33] For subsequent strokes, the AM and GM ratios of IEFP to OPO are 5.4 and 4.9 (5.2 and 4.8, if strokes at distances less than 50 km are excluded), respectively. These are appreciably larger than their first-stroke counterparts, with the AM value for the 50–350 km range being 5.2. The difference is probably related to different current and speed profiles along the first- and subsequent-stroke channels. Similar to first strokes, the distance dependence of the IEFP to OPO ratio is evident in Tables 3a, 3b and 3c.

4.3. Inferences on Lightning Interaction With the Ionosphere

[34] Here we interpret the initial positive half-cycle and the opposite-polarity overshoot of observed electric field waveforms as the ground wave and the second positive half-cycle as the one-hop ionospheric reflection (first sky wave), which is confirmed by finite difference time domain

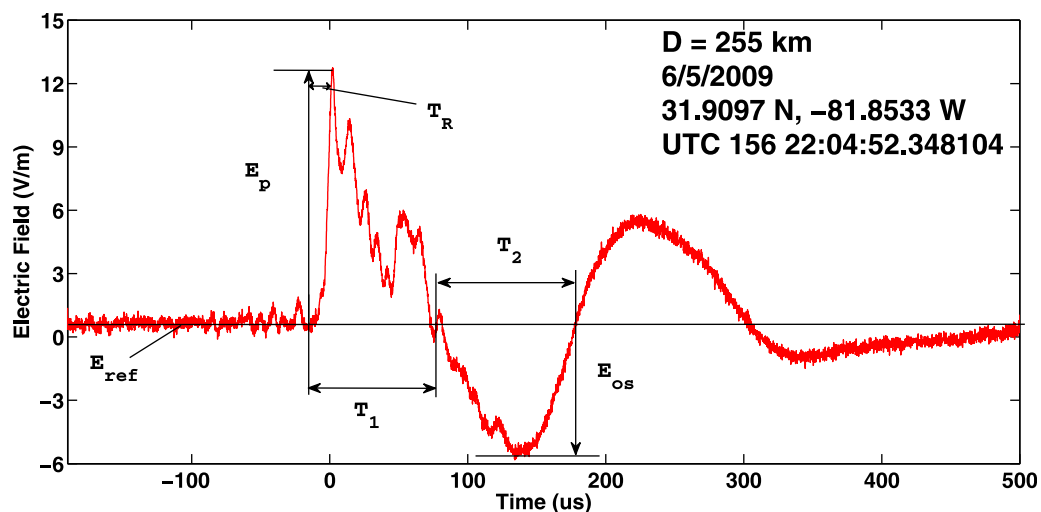


Figure 4. Definitions of the electric field waveform parameters.

Table 2a. The Arithmetic Mean for First Return Strokes Grouped Into Distance Ranges to Show the Dependence of Lightning Electric Field Waveform Features on Distance

Distance (km)	N	E_p (V/m)	E_{os} (V/m)	E_p/E_{os}	T_R (μ s)	T_1 (μ s)	T_2 (μ s)	$ I_{NLDN} $ (kA)	$ I $ (kA)	ΔI (%)
0–50 ^a	102	20.8	3.9 ^b	9.8 ^b	6.4	88.8 ^b	43.1 ^b	55.5	75.6	–25.6
50–100	54	29.9	9.4 ^c	4.4 ^c	8.4	95.7 ^c	117.4 ^c	92.2	109.3	–14.0
100–150	22	37.2	13.2	3.6	9.0	96.8	131.2	119.2	136.2	–11.9
150–200	29	33.8	12.2	3.1	8.5	84.2	127.5	103.7	123.6	–14.6
200–250	34	32.1	13.5	3.3	8.7	83.5	105.7	90.8	117.3	–18.8
250–300	17	39.3	19.2	2.2	8.5	78.7	104.4	108.4	143.8	–21.6
300–350 ^d	7	39.0	16.4	3.0	7.3	80.0	91.3	112.9	142.7	–20.2
10–330	265	28.6	11.6	4.3	7.7	88.6	107.1	83.0	104.2	–19.6
50–330	163	33.4	12.7	3.5	8.5	88.6	116.2	100.2	122.2	–15.9

^aThe smallest distance was 10 km.

^bThe tabulated value shown was determined for 20 out of the 102 recorded events; for the other 82 events this parameter was not measurable.

^cThe tabulated value shown was determined for 48 out of the 54 recorded events; for the other 6 events this parameter was not measurable.

^dThe largest distance was 330 km.

(FDTD) modeling results presented in Appendix A. Based on this interpretation, we compare differences in arrival times of the ground and first sky waves for first and subsequent strokes and corresponding effective ionospheric reflection heights.

[35] Essentially all field records examined here were acquired under daytime conditions. As a result, (a) the effective height of the ionospheric D region (responsible for reflection of VLF, 3–30 kHz, and LF, 30–300 kHz, radio waves) was relatively low and (b) it was much poorer (lossier) reflector than at night. The lower effective daytime ionosphere height (due to ionization by solar extreme ultraviolet photons) leads to a smaller time separation between the first sky wave and the ground one, and the higher losses make the shape of the sky wave much smoother than the ground wave, so that the former one appears to be seamlessly merged into the tail of the latter one. Ionospheric reflections in subsequent-stroke field waveforms are considerably less pronounced, probably due to their larger higher-frequency content [Serhan *et al.*, 1980], which is preferentially attenuated by the daytime ionosphere.

[36] Since, as opposed to nighttime waveforms, no breakpoint that signifies the instant of arrival of the first sky wave is discernible in our daytime field signatures, we assume that the sum of T_1 and T_2 (see Figure 4 and Tables 2a, 2b, 2c, 3a, 3b and 3c) roughly represents the difference in times of

arrival of the ground wave and the first sky wave. An alternative measure could be the time interval between the peaks of ground and first sky waves (peak-to-peak, as opposed to zero-to-zero, time). However, the peak-to-peak times may be inaccurate because of the very large dispersion of the sky wave relative to the ground wave under daytime conditions (see Figure A1 in Appendix A). On the other hand, finding the true zero time for the sky wave is virtually impossible. As noted in Appendix A, for the simulated electric field waveforms at distances ranging from 100 to 400 km, both peak-to-peak and zero-to-zero time differences are in general agreement with the simple time-of-flight predictions.

[37] Our assumption that the starting point of the first sky wave approximately corresponds to the second zero-crossing time (at $T_1 + T_2$) would be justified, if the errors involved were independent of the stroke order. In this case, even though the reflecting height might be in error, the difference in heights for first and subsequent strokes (the main finding of this section) is still valid. It is conceivable that the subsequent-stroke ground wave is shorter than its first-stroke counterpart and tends to produce the second zero-crossing earlier (before the arrival of the first sky wave). If so, some of the apparent difference in reflecting heights for first and subsequent strokes could be due to this effect, and the difference in reflecting heights is actually smaller. It is known that the initial positive half-cycle (not affected by

Table 2b. The Geometric Mean for First Return Strokes Grouped Into Distance Ranges to Show the Dependence of Lightning Electric Field Waveform Features on Distance

Distance (km)	N	E_p (V/m)	E_{os} (V/m)	E_p/E_{os}	T_R (μ s)	T_1 (μ s)	T_2 (μ s)	$ I_{NLDN} $ (kA)	$ I $ (kA)
0–50 ^a	102	18.0	2.5 ^b	8.7 ^b	6.04	80.1 ^b	22.4 ^b	45.2	65.0
50–100	54	28.0	6.8 ^c	3.8 ^c	7.8	92.1 ^c	107.6 ^c	83.9	102.2
100–150	22	34.5	10.9	3.2	8.5	93.6	127.9	106.7	126.0
150–200	29	32.0	11.0	2.9	7.8	83.0	126.6	92.0	116.8
200–250	34	30.2	10.6	2.8	8.1	82.1	103.7	83.2	110.0
250–300	17	37.1	17.2	2.2	8.2	78.0	104.1	96.9	135.7
300–350 ^d	7	38.7	14.6	2.6	6.1	79.3	89.6	107.1	141.6
10–330	265	25.3	8.4	3.5	7.1	85.5	91.4	69.1	91.9
50–330	163	31.3	10.0	3.1	7.9	86.2	111.4	90.2	114.2

^aThe smallest distance was 10 km.

^bThe tabulated value shown was determined for 20 out of the 102 recorded events; for the other 82 events this parameter was not measurable.

^cThe tabulated value shown was determined for 48 out of the 54 recorded events; for the other 6 events this parameter was not measurable.

^dThe largest distance was 330 km.

Table 2c. The Standard Deviation of the Logarithm (Base 10) of Each Parameter for First Return Strokes Grouped Into Distance Ranges to Show the Dependence of Lightning Electric Field Waveform Features on Distance

Distance (km)	N	E_p (V/m)	E_{os} (V/m)	E_p/E_{os}	T_R (μ s)	T_1 (μ s)	T_2 (μ s)	$ I_{NLDN} $ (kA)	$ I $ (kA)
0–50 ^a	102	0.24	0.40 ^b	0.22 ^b	0.16	0.21 ^b	0.60 ^b	0.29	0.24
50–100	54	0.16	0.49 ^c	0.22 ^c	0.19	0.12 ^c	0.21 ^c	0.20	0.17
100–150	22	0.18	0.28	0.24	0.14	0.11	0.11	0.22	0.19
150–200	29	0.15	0.21	0.15	0.16	0.07	0.05	0.23	0.15
200–250	34	0.15	0.30	0.21	0.17	0.08	0.09	0.20	0.15
250–300	17	0.14	0.20	0.13	0.11	0.06	0.04	0.23	0.14
300–350 ^d	7	0.06	0.23	0.23	0.29	0.06	0.09	0.17	0.06
10–330	265	0.22	0.42	0.26	0.18	0.11	0.34	0.28	0.23
50–330	163	0.16	0.36	0.21	0.17	0.10	0.14	0.21	0.16

^aThe smallest distance was 10 km.

^bThe tabulated value shown was determined for 20 out of the 102 recorded events; for the other 82 events this parameter was not measurable.

^cThe tabulated value shown was determined for 48 out of the 54 recorded events; for the other 6 events this parameter was not measurable.

^dThe largest distance was 330 km.

ionospheric reflections) for subsequent strokes is shorter than that for first strokes, but it is not clear if the true (not influenced by ionospheric reflections) durations of their opposite-polarity overshoots follow the same trend. A similar study under nighttime conditions, when sky wave signatures are more pronounced, can help resolve these issues.

[38] For first strokes at distances greater than 100 km, the zero-to-zero time between the ground and first sky waves is on average 201 μ s ($N = 108$), and for subsequent strokes it is 162 μ s ($N = 124$). Unfortunately, the University of Florida (UF) data reduction procedures were not optimal for studying ionospheric reflections. As a result, we cannot presently show the reduction in zero-to-zero time for subsequent strokes relative to the first stroke in the same flash. However, we do show here examples of waveforms recorded with a pair of magnetic field coils operating near Duke University with a bandwidth of approximately 100 Hz to 25 kHz. The latter is significantly lower than the upper frequency response (at least 10 MHz) of the UF measuring system, but the ionospheric influence on the waveforms is readily seen.

[39] Using NLDN data, we selected a group of 13 multistroke negative polarity lightning flashes that were between 200 and 400 km from the Duke sensors and that occurred during daylight hours (14:40 to 16:40 UT). The date (29 August 2011) was arbitrarily selected as one that had lightning strokes at the proper range. Visual inspection

shows that at least 10 of these flashes exhibit spheric waveforms with second peaks that are distinctly earlier for most or all subsequent strokes when compared to the first stroke. Figure 7 presents the waveforms for the two of these flashes that most clearly exhibit systematic differences between the first and subsequent stroke waveforms. The waveforms are normalized to unit peak amplitude for easier comparison. Figure 7 (top) shows the azimuthal magnetic field waveforms from a three-stroke flash at 16:23:27 UT at a range of 171 km from the sensor. Figure 7 (bottom) is similar, but for a five-stroke flash at 14:51:30 UT at a range of 304 km. In both cases, the first stroke waveform exhibits a second peak that is significantly later in time by several tens of microseconds than any of the subsequent stroke waveforms, in support of the UF data. This shows that the phenomenon is observable in the waveforms from individual flashes and not just in a statistical comparison of first and subsequent strokes.

[40] Subsequent-stroke electromagnetic signals are expected to be reflected at more or less the same height as their corresponding first-stroke signals, which should lead to the same difference in times of arrival of the ground wave and the first sky wave. The observed disparity between the first and subsequent strokes in terms of the arrival time of the first sky wave relative to the ground one implies a lower effective ionosphere height for subsequent strokes. We calculated the

Table 3a. Same as Table 2a but for Subsequent Strokes

Distance (km)	N	E_p (V/m)	E_{os} (V/m)	E_p/E_{os}	T_R (μ s)	T_1 (μ s)	T_2 (μ s)	$ I_{NLDN} $ (kA)	$ I $ (kA)	ΔI (%)
0–50 ^a	152	10.2	1.2 ^b	7.4 ^b	4.6	58.2 ^b	19.8 ^b	25.9	36.4	–30.1
50–100	68	10.2	2.2 ^c	6.7 ^c	5.0	70.8 ^c	64.0 ^c	28.8	36.3	–21.6
100–150	28	11.6	2.4	5.8	4.9	71.8	91.5	30.8	41.6	–25.9
150–200	37	10.9	2.5	4.6	5.0	67.2	105.2	29.8	38.7	–22.9
200–250	47	12.1	3.2	4.2	5.9	65.7	95.7	32.9	43.3	–24.3
250–300	11	11.5	3.1	4.1	4.0	63.8	74.7	29.6	41.2	–26.0
300–350 ^d	6	12.9	3.9	3.5	4.0	73.8	69.4	39.0	46.1	–17.3
10–330	349	10.8	2.6	5.4	5.0	67.6	80.4	28.6	38.3	–26.2
50–330	197	11.1	2.7	5.2	5.1	68.5	86.1	30.6	39.7	–23.2
$ I_{NLDN} > 50$ kA	35	19.4	5.0	5.2	6.4	82.2	117.1	63.1	71.0	–9.6

^aThe smallest distance was 10 km.

^bThe tabulated value shown was determined for 16 out of the 152 recorded events; for the other 136 events this parameter was not measurable.

^cThe tabulated value shown was determined from 49 out of the 68 recorded events; for the other 19 events this parameter was not measurable.

^dThe largest distance was 330 km.

Table 3b. Same as Table 2b but for Subsequent Strokes

Distance (km)	N	E_p (V/m)	E_{os} (V/m)	E_p/E_{os}	T_R (μ s)	T_1 (μ s)	T_2 (μ s)	$ I_{NLDN} $ (kA)	$ I $ (kA)
0–50 ^a	152	9.0	1.0 ^b	7.3 ^b	4.1	54.6 ^b	15.1 ^b	22.1	31.9
50–100	68	9.6	1.7 ^c	6.1 ^c	4.4	64.1 ^c	39.0 ^c	25.7	33.7
100–150	28	10.4	2.1	5.3	4.7	66.6	67.0	26.3	36.6
150–200	37	10.2	2.3	4.5	4.8	60.7	88.3	26.9	36.1
200–250	47	11.3	2.9	4.0	5.2	58.7	84.5	28.9	40.1
250–300	11	10.7	2.9	3.9	3.7	60.0	69.8	26.3	38.0
300–350 ^d	6	12.4	3.7	3.3	3.7	70.7	65.1	35.2	44.1
10–330	349	9.7	2.1	4.9	4.4	61.5	57.5	24.8	34.4
50–330	197	10.3	2.3	4.8	4.6	62.2	65.0	27.0	36.6
$ I_{NLDN} > 50$ kA	35	19.1	4.1	4.5	5.8	77.8	106.6	62.0	69.1

^aThe smallest distance was 10 km.

^bThe tabulated value shown was determined for 16 out of the 152 recorded events; for the other 136 events this parameter was not measurable.

^cThe tabulated value shown was determined from 49 out of the 68 recorded events; for the other 19 events this parameter was not measurable.

^dThe largest distance was 330 km.

ionospheric reflection height, h_1 , for the first sky wave for first and subsequent strokes using the following equation [e.g., *Laby et al.*, 1940]:

$$h_1 = R_e \left[\cos^2 \left(\frac{D}{2R_e} \right) - 1 \right] + \sqrt{\left\{ R_e^2 \left[\cos^2 \left(\frac{D}{2R_e} \right) - 1 \right] + \left(\frac{ct_1 + D}{2} \right)^2 \right\}} \quad (8)$$

where $R_e = 6367$ km is the mean radius of the Earth, D is the distance to the lightning channel, t_1 is the difference in arrival times of the first sky wave and the ground wave, and c is the speed of light. As noted earlier, we assume here that $t_1 = T_1 + T_2$ (see Figure 4). Histograms of the reflection heights h_1 for first and subsequent strokes (all at distances greater than 100 km) are shown in Figures 8a and 8b, respectively. The corresponding scatterplots of h_1 versus distance are shown in Figures 9a and 9b. Clearly, there is more scatter for subsequent strokes than for the first ones. This is possibly indicative of lower ionosphere that is perturbed to a various degree at times when subsequent strokes occur. The arithmetic means of h_1 for first and subsequent strokes are 81 and 70 km, respectively (Table 4), corresponding to an ionosphere descent of 11 km. The corresponding standard errors are 0.69 km and 1.3 km, in both cases less than 2% of the mean value. The histogram for subsequent strokes exhibits a long tail extending to heights as

low as 30 km, considerably lower than the mean of 70 km (possibly making the standard-error measure not applicable). There is no similar tail in the histogram for first strokes, which resembles a Gaussian distribution. For most of the subsequent strokes (103 out of 124 or 83%) the mean reflection height is about 76 km, which is about 5 km lower than that for the first strokes. We speculate that the abnormally low reflection heights in Figures 8b and 9b correspond to higher-order subsequent strokes, prior to which there was cumulative effect in lowering ionosphere by multiple lower-order strokes. In this view, the main part of the histogram for subsequent strokes corresponds to lower-order strokes, for which there is little or no cumulative effect. Clearly, more studies are needed to verify these inferences.

[41] Interestingly, the effective reflecting height for subsequent strokes, 70 km, is similar to the expected height of the daytime ionosphere [*Smith et al.*, 2004, Figure 6], while that for first strokes, 81 km, is somewhat larger. The apparent overestimation of reflection heights might be related to a tendency for our method to yield larger differences in arrival times of the ground wave and first sky wave relative to simple time-of-flight predictions, seen for larger distances in Table A1 in Appendix A. This tendency can also be responsible for the increasing trends in the h_1 versus D plots shown in Figures 9a and 9b. As noted earlier, even if our absolute heights are in error (overestimates), the difference in heights for first and subsequent strokes, which is the main finding of this section, should still hold.

Table 3c. Same as Table 2c but for Subsequent Strokes

Distance (km)	N	E_p (V/m)	E_{os} (V/m)	E_p/E_{os}	T_R (μ s)	T_1 (μ s)	T_2 (μ s)	$ I_{NLDN} $ (kA)	$ I $ (kA)
0–50 ^a	152	0.29	0.19 ^b	0.10 ^b	0.20	0.17 ^b	0.33 ^b	0.26	0.28
50–100	68	0.16	0.27 ^c	0.21 ^c	0.22	0.20 ^c	0.48 ^c	0.21	0.17
100–150	28	0.22	0.23	0.17	0.14	0.17	0.38	0.25	0.23
150–200	37	0.15	0.18	0.13	0.13	0.20	0.32	0.20	0.16
200–250	47	0.16	0.20	0.15	0.20	0.20	0.26	0.23	0.17
250–300	11	0.17	0.16	0.13	0.14	0.17	0.19	0.23	0.18
300–350 ^d	6	0.13	0.15	0.15	0.19	0.14	0.18	0.23	0.14
10–330	349	0.23	0.25	0.19	0.20	0.19	0.42	0.24	0.23
50–330	197	0.17	0.24	0.18	0.19	0.19	0.38	0.22	0.18
$ I_{NLDN} > 50$ kA	35	0.08	0.25	0.25	0.19	0.15	0.20	0.08	0.08

^aThe smallest distance was 10 km.

^bThe tabulated value shown was determined for 16 out of the 152 recorded events; for the other 136 events this parameter was not measurable.

^cThe tabulated value shown was determined from 49 out of the 68 recorded events; for the other 19 events this parameter was not measurable.

^dThe largest distance was 330 km.

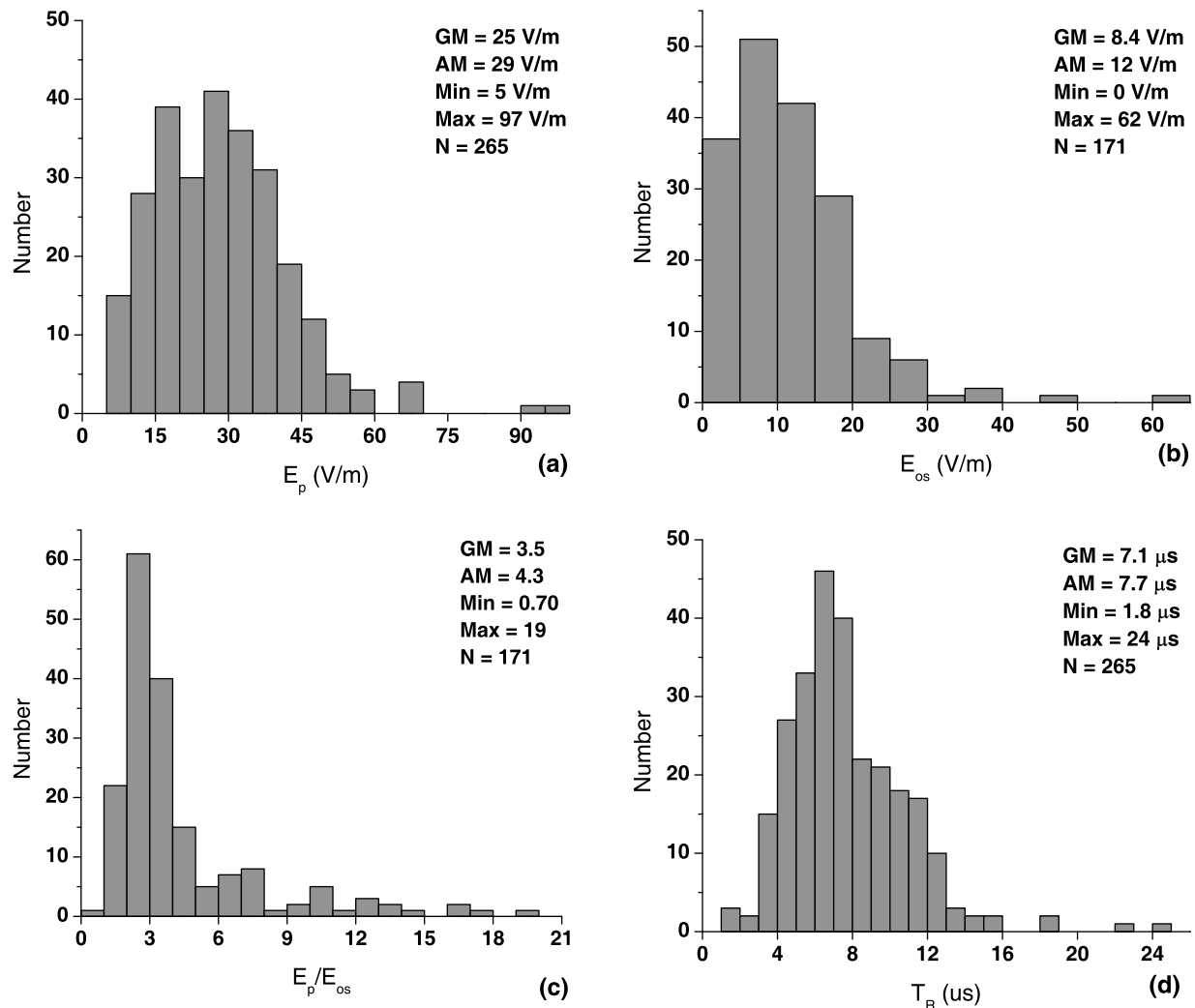


Figure 5. Histograms of field waveform parameters and estimated currents for all first strokes regardless of distance: (a) E_p , (b) E_{os} , (c) E_p/E_{os} , (d) T_R , (e) T_1 , (f) T_2 , (g) $|I_{NLDN}|$, (h) $|I|$, (i) ΔI .

[42] One possible explanation of the apparent descent of the ionosphere after the first stroke is interaction of the electromagnetic signal of the first stroke with the ionosphere [e.g., Rowland *et al.*, 1996; Rakov and Tuni, 2003], which temporarily modifies it so that the electromagnetic signal of a following stroke is reflected at a lower altitude. There is a large body of literature on simulations and measurements of ionospheric perturbations caused by strong cloud-to-ground discharges and bursts of cloud-discharge pulses [e.g., Inan *et al.*, 1991; Taranenko *et al.*, 1993; Cheng and Cummer, 2005; Cheng *et al.*, 2007; Kumar *et al.*, 2008; Marshall *et al.*, 2010]. A good review is given by Inan *et al.* [2010]. Lightning-driven mechanisms that are known to perturb the ionosphere are elves expanding over a radial distance of up to a few hundred kilometers across the bottom of the ionosphere, halos occurring below elves altitudes, and sprites, extending between 40 and 90 km heights and often having faint tendrils extending from 50 km or so to altitudes as low as 20 km (near the cloud tops). The discharges analyzed here are of negative polarity and thus

very likely not to have created sprites. Lightning interactions with the ionosphere are relatively brief (for example, optical elves typically last less than 1 ms), but their effects can persist for 10–100 s [e.g., Inan *et al.*, 2010], which is much longer than the duration of causative lightning flash.

[43] Elves and halos are known to create ionospheric height perturbations of several kilometers during nighttime conditions [Inan *et al.*, 2010], which is smaller than the mean value of 11 km inferred in this study for all subsequent strokes, but comparable to that of 5 km for the majority (83%) of those strokes. It should be emphasized that the previously studied lightning perturbations are almost exclusively for nighttime conditions, because of the visibility of the associated optical emissions. To our knowledge, localized lightning-driven ionospheric perturbations have not been studied under daytime conditions. The magnitude of the apparent height changes found here is rather large, but this could be due to cumulative contributions of multiple strokes to lowering the ionospheric reflection height. Further investigation is clearly needed to verify our interpretation of differences

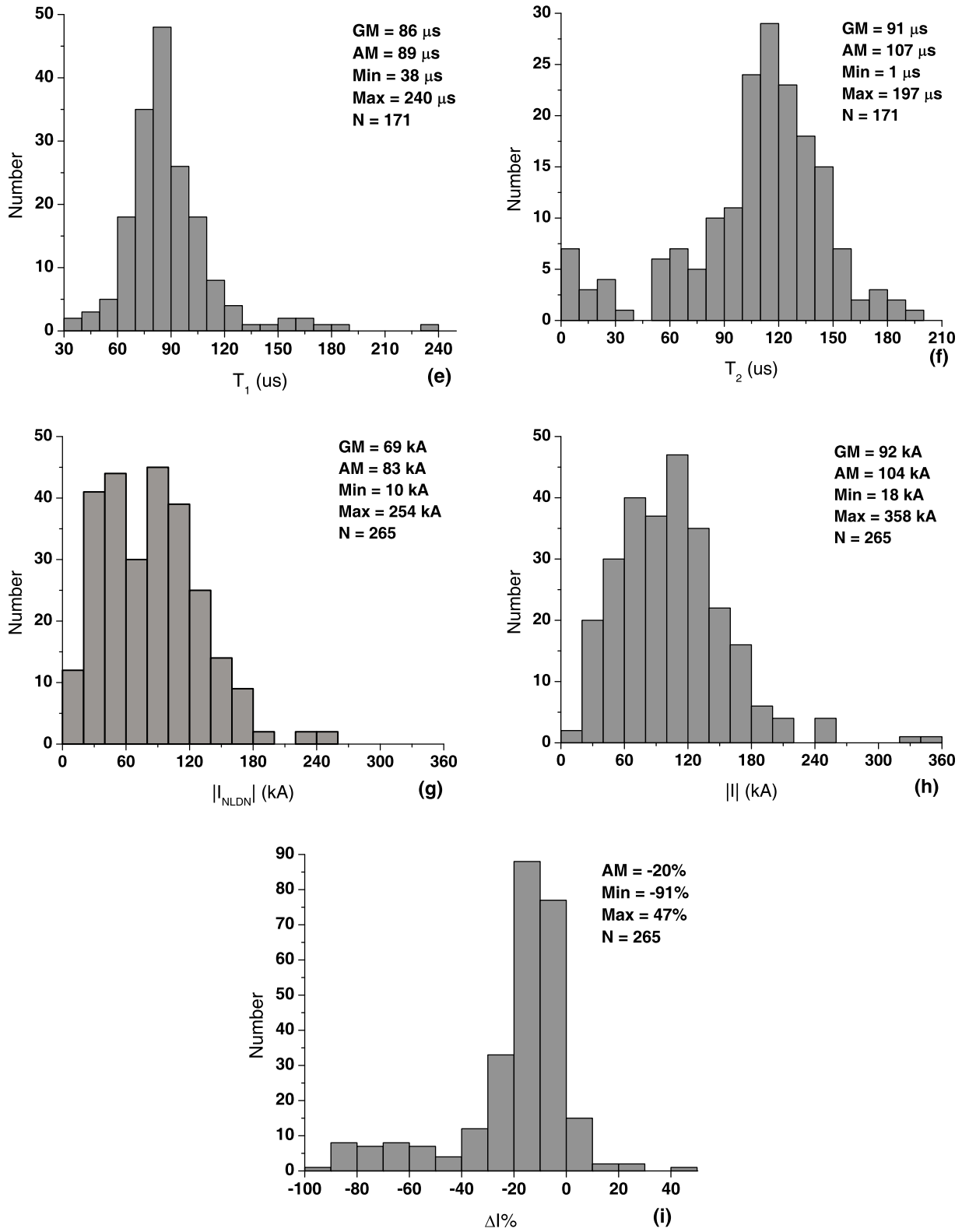


Figure 5. (continued)

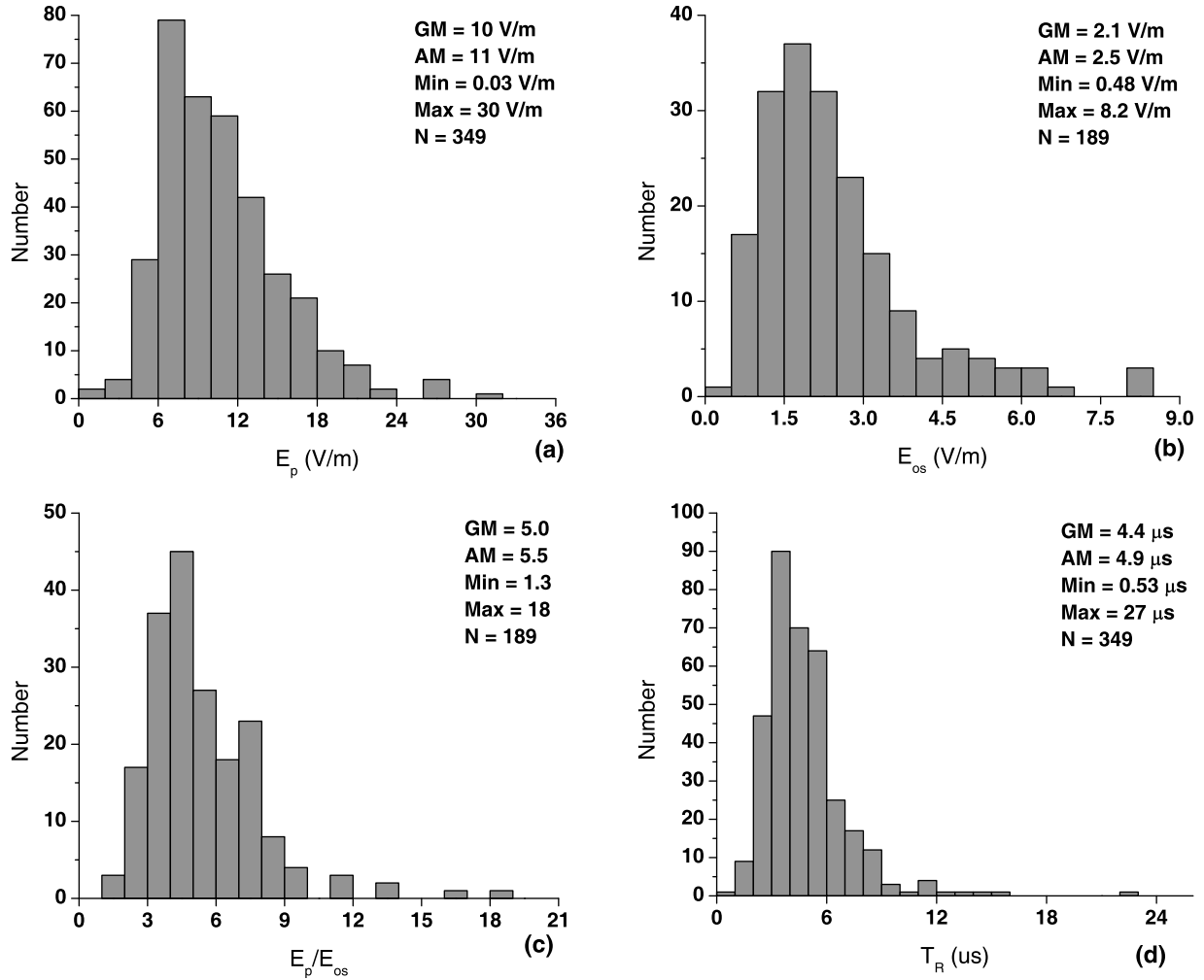


Figure 6. Histograms of field waveform parameters and estimated currents for all subsequent strokes regardless of distance: (a) E_p , (b) E_{os} , (c) E_p/E_{os} , (d) T_R , (e) T_1 , (f) T_2 , (g) $|I_{NLDN}|$, (h) $|I|$, (i) ΔI .

in daytime field waveforms produced by first and subsequent strokes at distances ranging from 100 and 330 km.

4.4. Peak Current Estimates

[44] Peak currents estimated from the empirical formula, as well as NLDN-reported peak currents, are biased toward larger values for the reasons discussed in section 4.2.1. For all first and subsequent strokes, the GM peak currents from the empirical formula are 92 and 34 kA, respectively, versus typical [e.g., Rakov and Uman, 2003] 30 and 10–15 kA, respectively. The corresponding NLDN-reported values are 69 and 25 kA.

[45] The arithmetic mean values of percent difference ΔI between the NLDN-reported current and that estimated from the empirical formula, computed from equation (6), for first and subsequent strokes are -20% and -26% , respectively (see Figures 5i and 6i). This means that the NLDN-reported peak current is on average about 20% lower than that predicted by the empirical formula for first strokes and about 26% lower for subsequent strokes. Further, the distribution of ΔI for both first and subsequent strokes appears to be bimodal: besides the primary peak around -20% , there is an additional one around -70% for first strokes (Figure 5i) and -60% for subsequent strokes (Figure 6i). This additional

peak is more pronounced for subsequent strokes, although for both types of strokes it may be viewed as a hump on a long tail approaching -100% . In contrast, positive values of ΔI do not exceed 50%.

[46] The NLDN is known to underestimate lightning peak currents, as determined from direct current measurements for triggered-lightning strokes [Jerould *et al.*, 2005; Nag *et al.*, 2011a; Mallick *et al.*, 2011], which are similar to subsequent strokes in natural lightning. Also, Pavlick *et al.* [2002] found that the NLDN-reported peak currents for first strokes (prior to the 2004 upgrade) were on average about 10% lower than those predicted by the empirical formula (they excluded from their analysis a few events for which there was “a gross difference” between the NLDN-reported and empirical-formula-predicted peak currents, assuming that those events were misidentified in the NLDN data). Underestimation of peak currents by the NLDN is usually attributed to undercompensated field propagation effects and limited upper frequency response of the NLDN (discussed below). On the other hand, the peak-current estimates from the empirical formula do not constitute the absolute ground-truth, and NLDN-estimated peak currents after July 1, 2004 (when the field propagation model was changed from the power law to

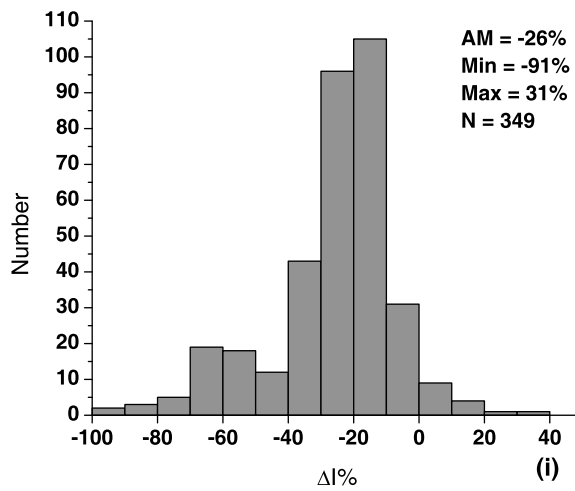
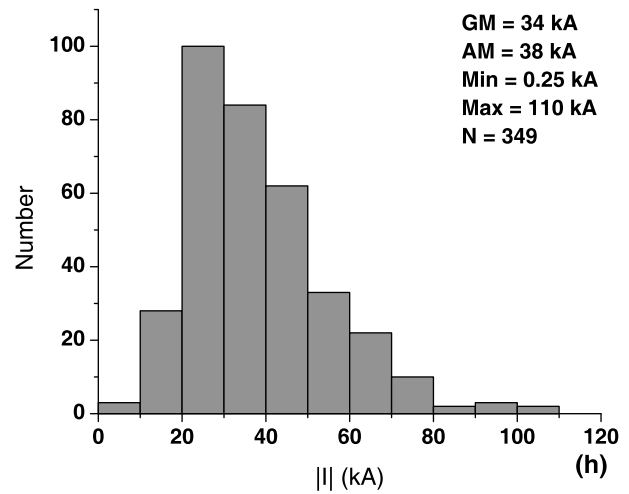
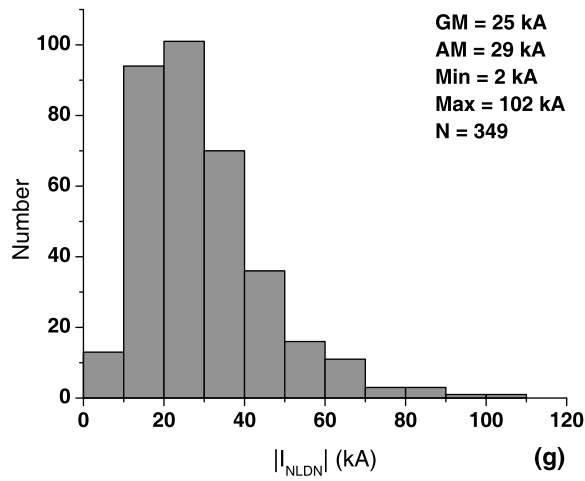
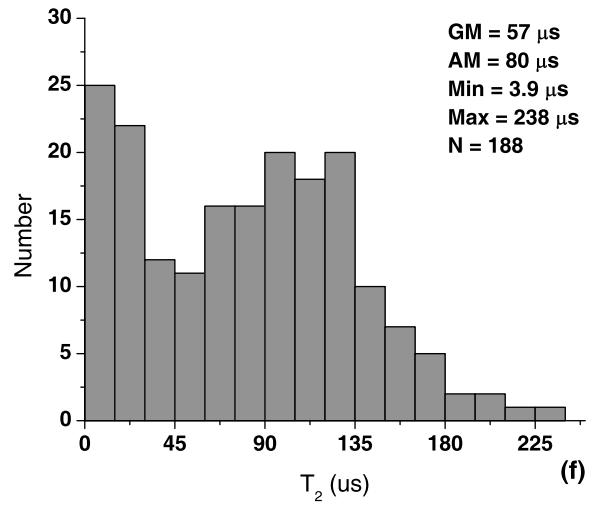
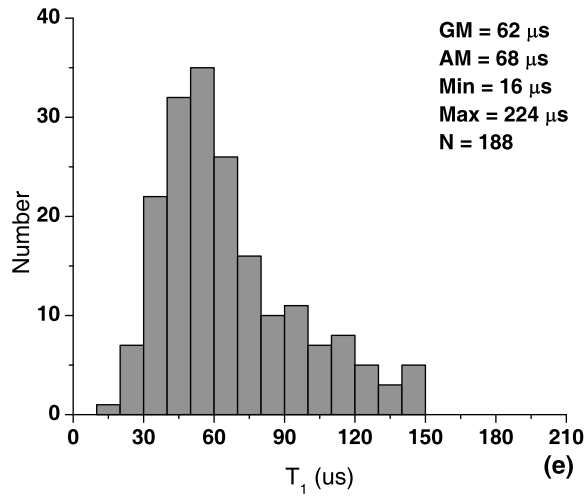


Figure 6. (continued)

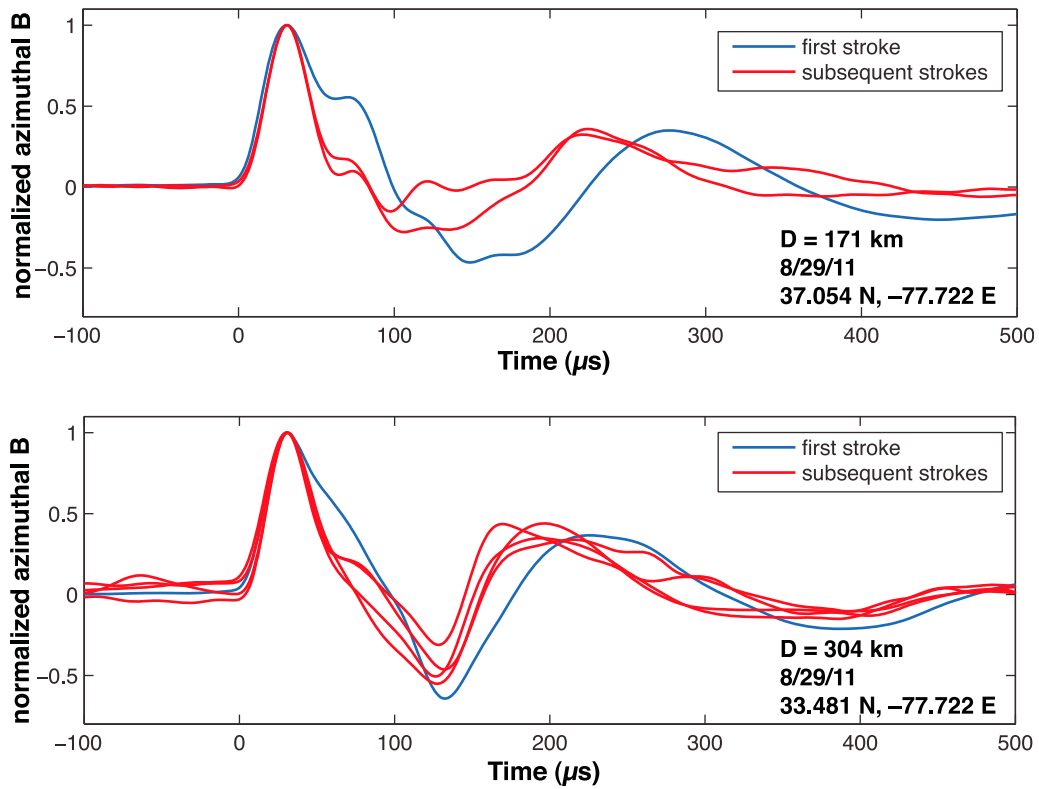


Figure 7. Illustration of the reduction of the difference in times of arrival of ground and first sky waves for subsequent strokes relative to the first stroke in the same flash. Shown here are the magnetic field waveforms recorded with a system having a bandwidth of 100 Hz to 25 kHz near Duke University. See text for details.

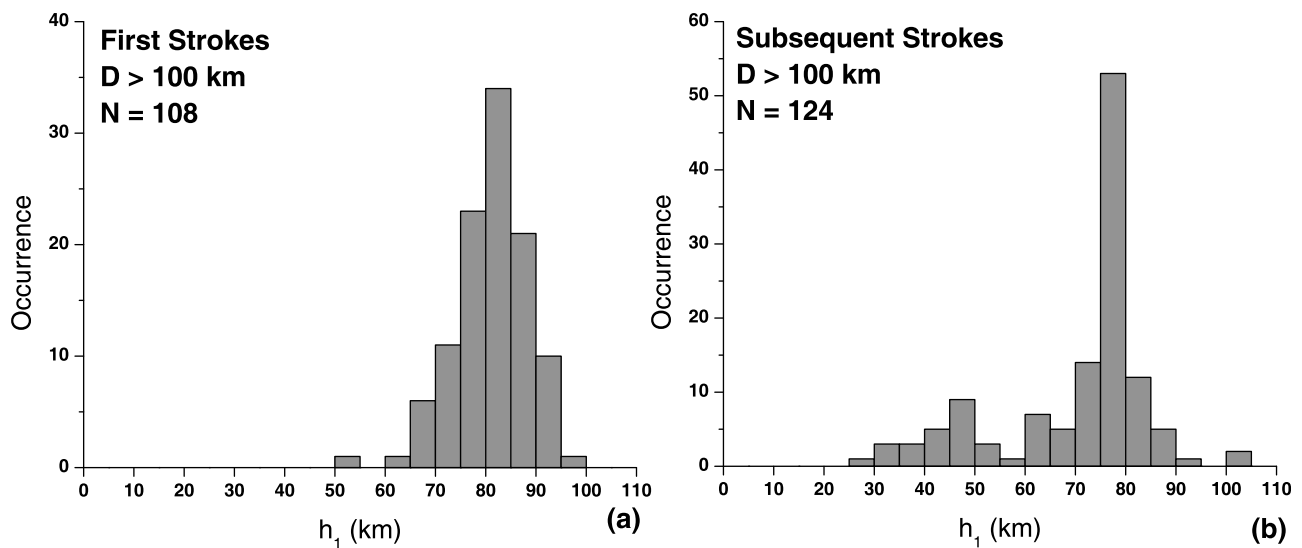


Figure 8. Histograms of ionospheric reflection heights h_1 for (a) first and (b) subsequent strokes, all at distances D greater than 100 km.

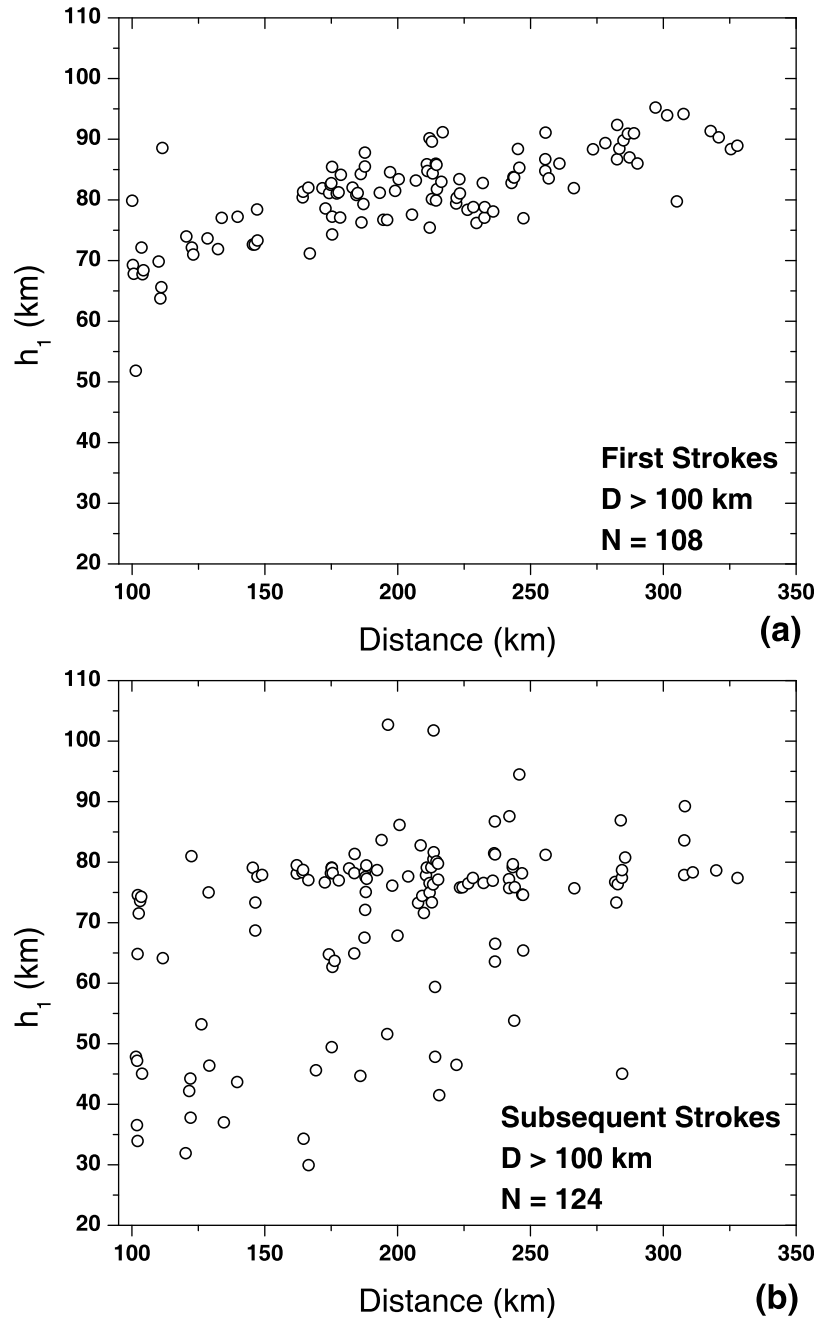


Figure 9. Scatterplots of h_1 versus D for (a) first and (b) subsequent strokes, all at distances greater than 100 km.

Table 4. Mean Values of t_1 and h_1 for First and Subsequent Strokes, All at Distances Greater Than 100 km

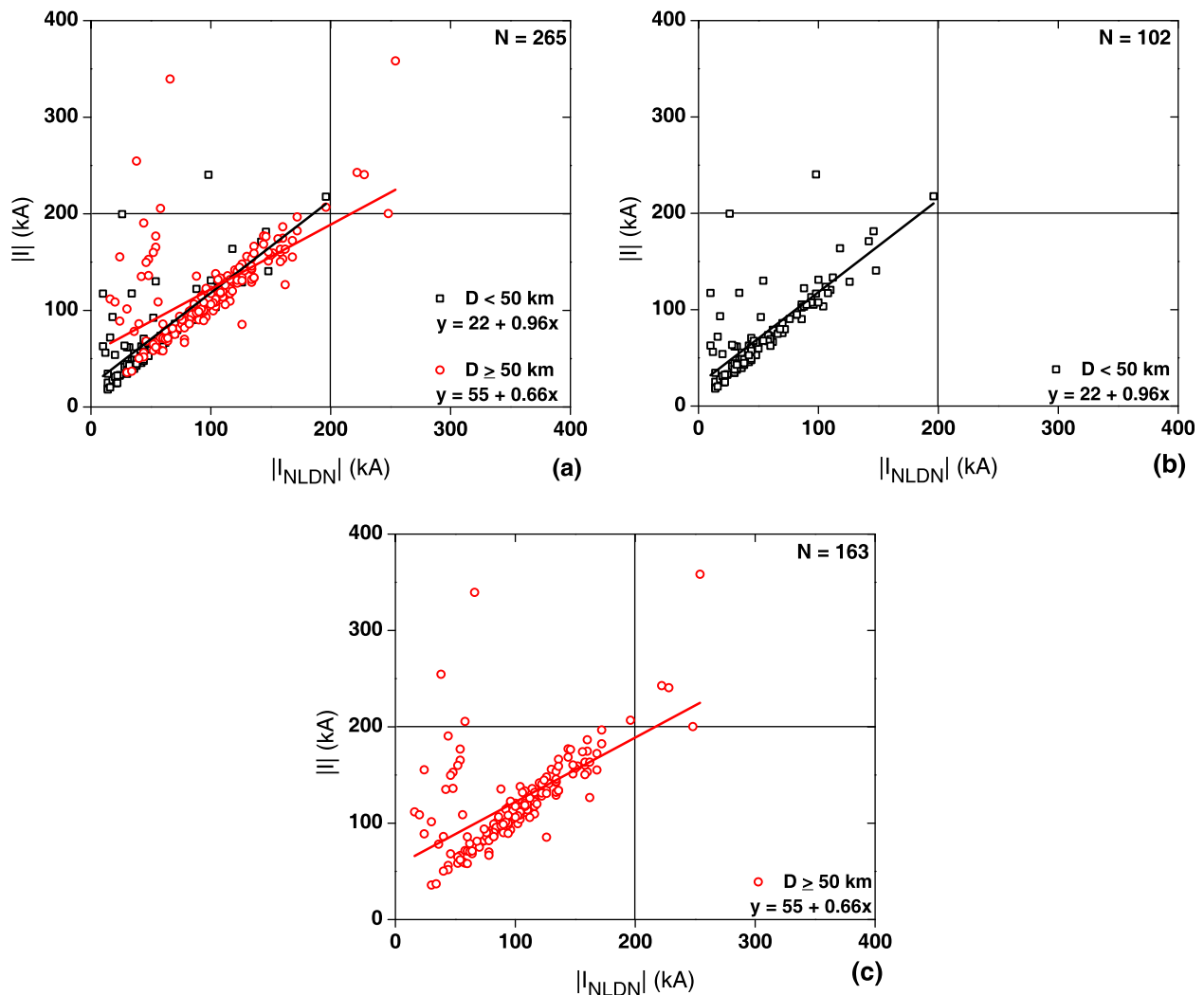
	Mean Values	
	$t_1 \approx T_1 + T_2$	h_1
First Strokes (n = 108)	200 μs	81 km
Subsequent strokes (n = 124)	162 μs	70 km

exponential) apparently show a smaller tendency to be underestimated [Nag *et al.*, 2011a]. Nevertheless, if we accept that the primary peak seen in Figures 5i and 6i is due to the known, kind of inherent NLDN tendency to underestimate peak currents, it appears that there is an additional source of appreciably larger errors in NLDN-reported currents, which is responsible for the secondary peak.

[47] One possible reason for NLDN underestimation of peak currents is its limited upper frequency response of about 400 kHz. We digitally low-pass filtered 44 representative first-stroke electric field waveforms from our data set using

a 4-pole Bessel filter having -6 -dB frequency of 400 kHz. The zero-to-peak risetimes varied from 2 to 22 μs with about equal number of events representing the shortest, longest, and intermediate risetimes. We believe that the results are representative of both first and subsequent strokes. The return-stroke waveforms after filtering became smoother, but their overall shape and primary fine structure were preserved. The initial peak was found to slightly decrease (by 4.8% on average, with the maximum decrease being less than 11%). This is in contrast with narrower electric field waveforms of compact intracloud lightning discharges (CIDs), whose peaks after similar filtering decreased by 9.1 to 41% [Nag *et al.*, 2011b].

[48] As noted above, the empirical formula cannot be viewed as absolute ground-truth for NLDN peak current estimates. It is based on data for triggered-lightning strokes and, therefore, strictly speaking, is applicable only to subsequent strokes. Further, those data are limited (only 28 events) and may be not representative even of triggered-lightning strokes in other experiments. Mallick *et al.* [2011] used electric fields of 91 rocket-triggered lightning strokes recorded (by a

**Figure 10.** Scatterplots of $|I_{NLDN}|$ versus $|I|$ for first strokes: (a) all distances, (b) $D < 50$ km, and (c) $D \geq 50$ km.

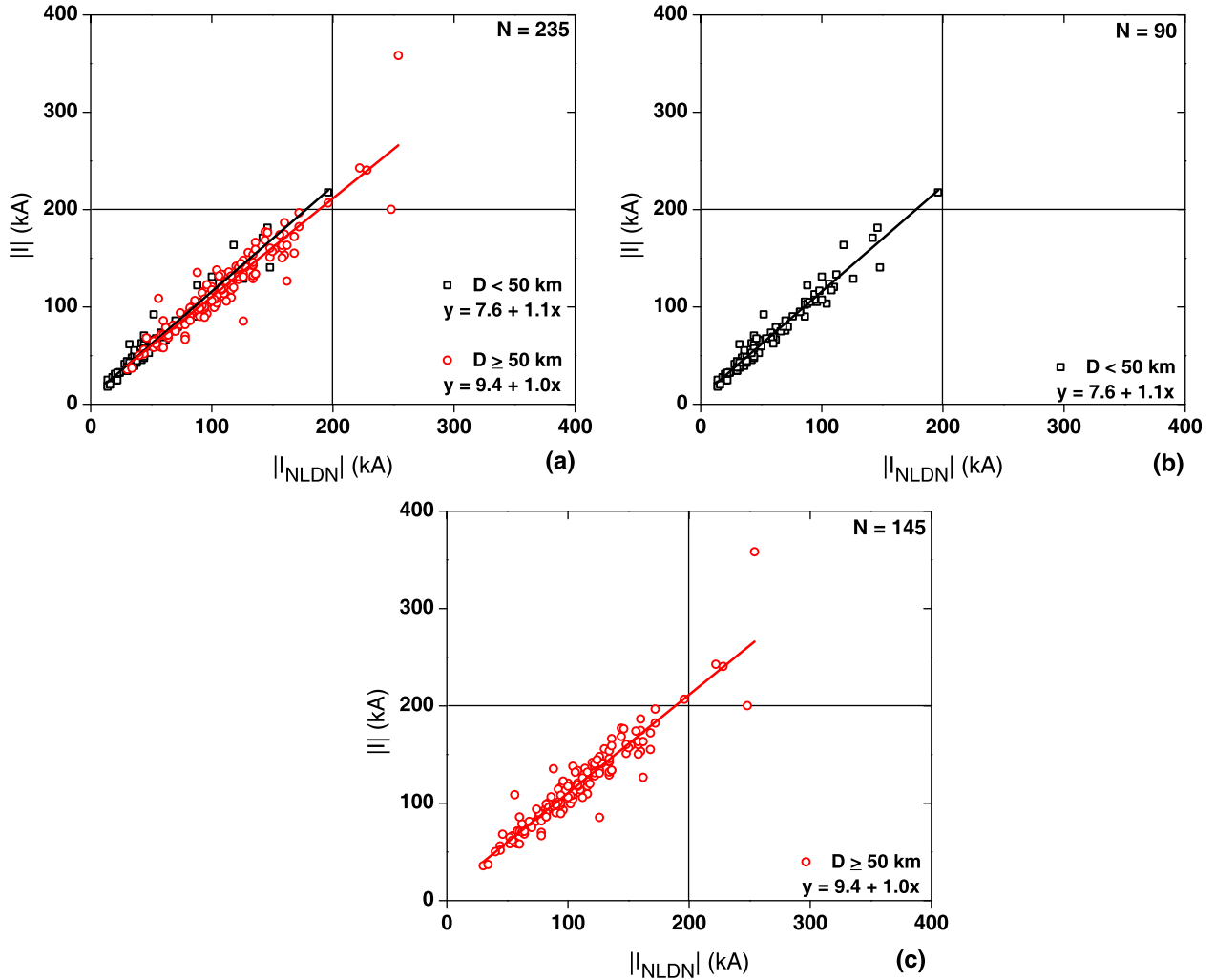


Figure 11. Scatterplots of $|I_{NLDN}|$ versus $|I|$ with $|\Delta I| < 50\%$ for first strokes: (a) all distances, (b) $D < 50$ km, and (c) $D \geq 50$ km.

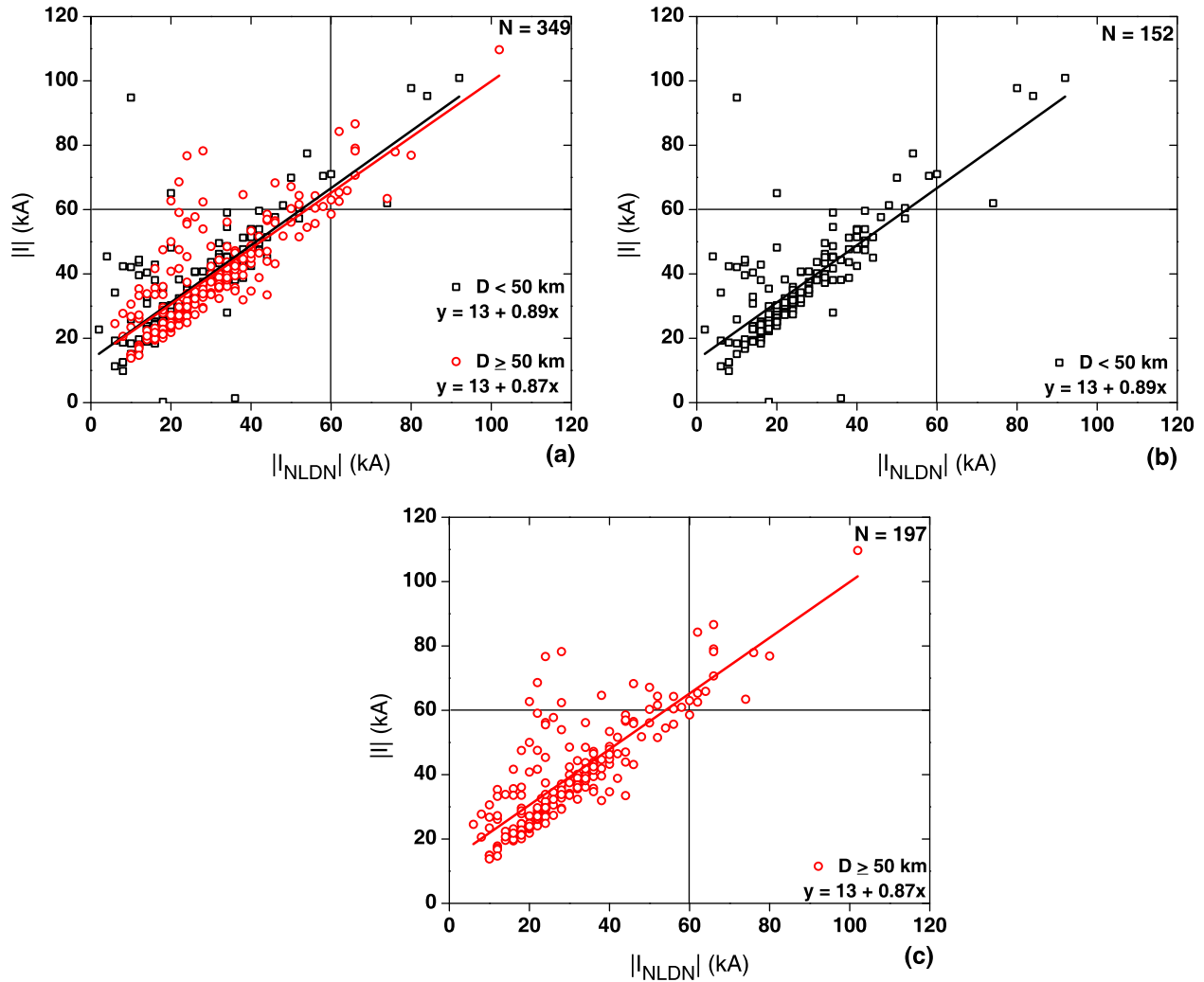


Figure 12. Scatterplots of $|I_{NLDN}|$ versus $|I|$ for subsequent strokes: (a) all distances (b) $D < 50$ km, and (c) $D \geq 50$ km.

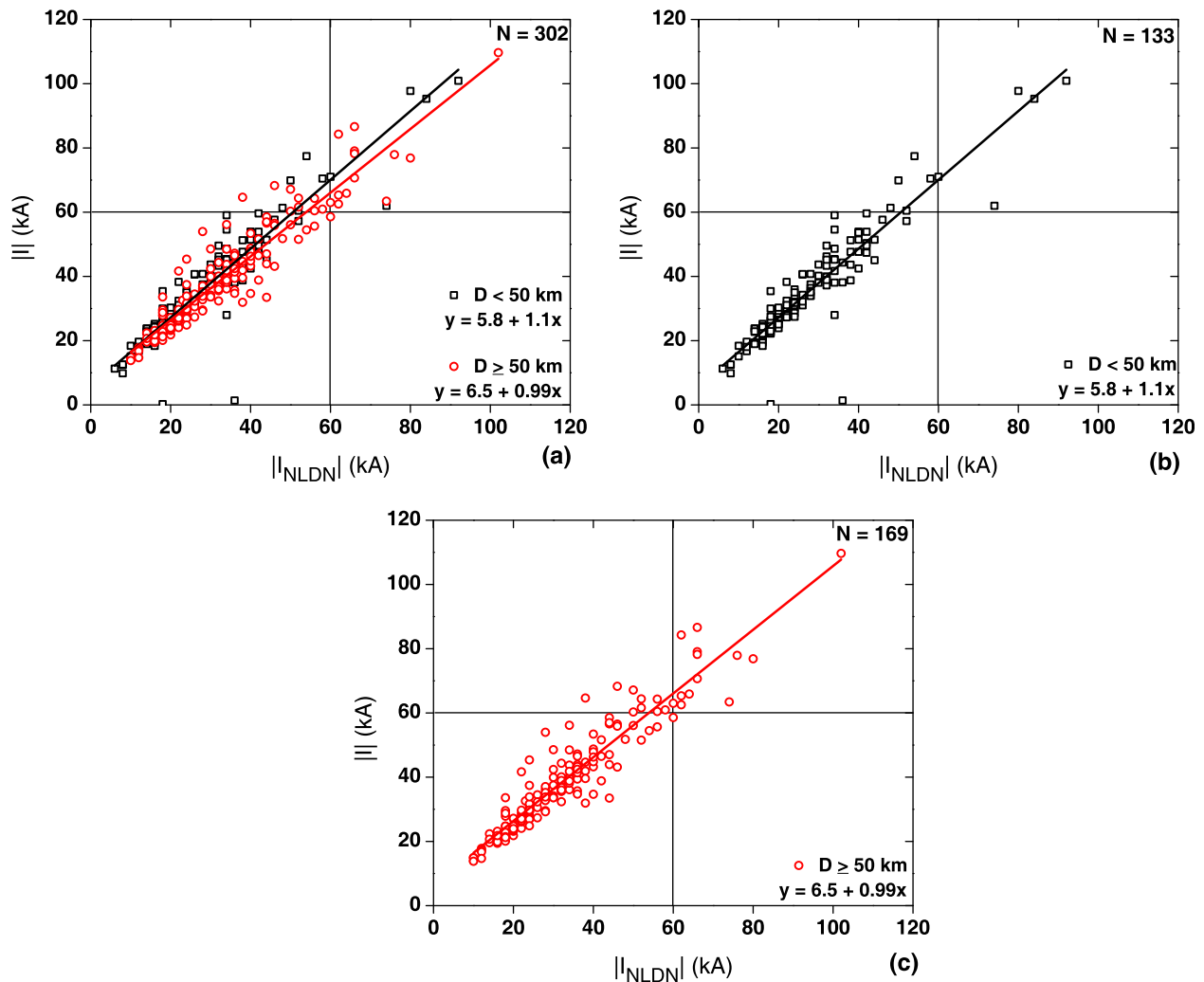


Figure 13. Scatterplots of $|I_{NLDN}|$ versus $|I|$ with $|\Delta I| < 50\%$ for subsequent strokes: (a) all distances, (b) $D < 50$ km, and (c) $D \geq 50$ km.

different, but similar system) at the LOG at a distance of about 45 km from the lightning channel to estimate peak currents from the empirical formula of *Rakov et al.* [1992] (equation (6) of this paper). The results were compared to the corresponding current peaks directly measured at the lightning channel base. They found that the empirical formula tended to overestimate peak currents, whereas the NLDN-reported peak currents were on average underestimates. The median value of ratios of directly measured and predicted by the empirical formula currents for the 91 strokes was found to be 0.85; that is, actual currents were on average 15% lower than those given by the empirical formula. *Mallick et al.* [2011] discussed two possible interpretations of this discrepancy. The first one is an error in the field calibration factor at LOG and the second one is a difference in typical return-stroke speeds in the 1987 KSC data (28 events), on which the empirical formula is based, and 2008–2010 Camp Blanding data (91 events) used by *Mallick et al.* [2011]. They additionally noted relatively small sample sizes, particularly for the KSC data.

[49] If we formally apply a “correction” factor of 0.85 to all the peak currents predicted by the empirical formula

in this study, the arithmetic mean values of ΔI for first and subsequent strokes will be -5.9% and -13% , respectively, while the positions of secondary peaks (humps) in ΔI distributions (see Figures 5i and 6i) will not change significantly.

[50] In summary, it appears that there is an additional source of discrepancy between I_{NLDN} and I resulting in $|\Delta I|$ equal to or greater than 50%. Perhaps the larger errors are associated with the NLDN misidentifying one of the step pulses (most likely the last one) as the return-stroke pulse. It is worth noting that the percentage of strokes exhibiting the larger discrepancies is relatively small.

[51] We now compare I_{NLDN} and I for all strokes without selection and only for those characterized by $|\Delta I| < 50\%$. Scatterplots of $|I|$ versus $|I_{NLDN}|$ for all first strokes and for those with $|\Delta I| < 50\%$ are shown in Figures 10 and 11, respectively. Scatterplots of $|I|$ versus $|I_{NLDN}|$ for all subsequent strokes and for those with $|\Delta I| < 50\%$ are shown in Figures 12 and 13, respectively. In all these Figures, we additionally included scatterplots for distances smaller and equal to or greater than 50 km. As expected, a good match

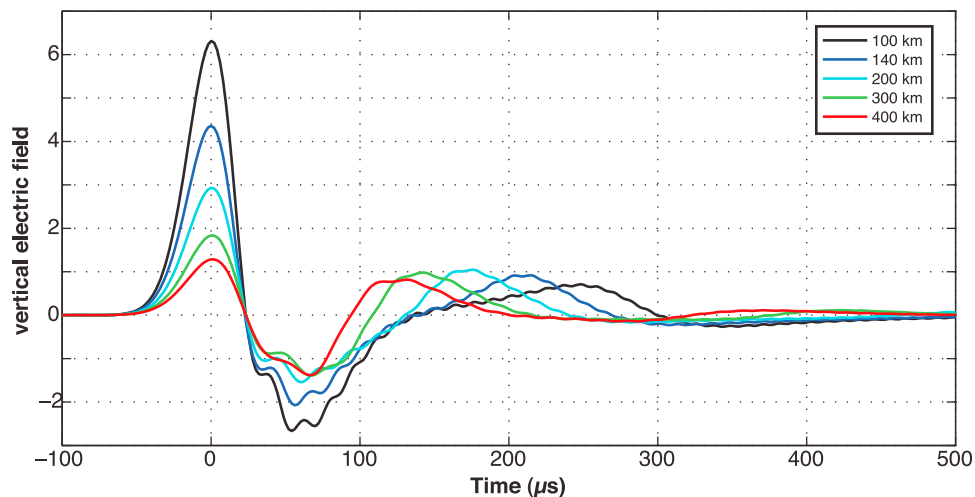


Figure A1. Simulated vertical electric field waveforms at distances ranging from 100 to 400 km. The second positive half-cycle, occurring at earlier times as the distance increases, is a reflection from the simulated daytime ionosphere. See text for details.

for both first and subsequent strokes is seen when the larger-discrepancy events are excluded.

5. Summary

[52] The overwhelming majority of both first and subsequent return-stroke electric field waveforms (96 and 88%, respectively) at 50 to 330 km exhibit an opposite polarity overshoot, expected for essentially radiation field waveforms. Geometric mean (GM) first zero-crossing times are 86 μs and 62 μs for first and subsequent strokes, respectively. The first zero-crossing times are longer than previously reported for Florida and Oklahoma, due to our use of better instrumentation. The corresponding GM ratios of the initial electric field peak to opposite polarity overshoot are 3.1 and 4.8. These results can be used in testing the validity of lightning return-stroke models.

[53] At distances greater than 100 km, electric field waveforms, recorded under daytime conditions, tend to be oscillatory, showing two cycles within 500 μs , with the corresponding frequency being about 4–5 kHz. The initial positive half-cycle and the opposite polarity overshoot are the ground wave and the second positive half-cycle is the one-hop ionospheric reflection, as confirmed by FDTD modeling. The observed difference in arrival times of these two waves for subsequent strokes is considerably smaller than for first strokes, suggesting that the first-stroke electromagnetic field caused a descent of the lower ionosphere. For most (103 out of 124) of the subsequent strokes the mean reflection height is about 76 km, which is about 5 km lower than that for the first strokes, but the height distribution exhibited a long tail, extending to as low as 30 km. We speculate that there may be cumulative contributions of multiple strokes to lowering the ionospheric reflection height. For all subsequent strokes combined, the mean reflection height is 70 km, which is 11 km lower than that for first strokes. The observed effect may be specific to the daytime ionosphere and high-intensity strokes that dominate our data set. Clearly, further studies are needed.

[54] The NLDN-reported current, I_{NLDN} , is on average about 20% lower than that predicted by the empirical formula, I , for first strokes and about 26% lower for subsequent strokes. It appears that there are two sources of discrepancy, ΔI , between I and I_{NLDN} , the primary one resulting in typical values of $|\Delta I|$ of about 20% and an additional one resulting in $|\Delta I|$ equal to or greater than 50%.

Appendix A

[55] Here we present the results of very low frequency (with an upper frequency limit of about 30 kHz) sferic propagation simulations to conclusively demonstrate that the second positive half-cycle feature, that is the focus of the analysis in section 4.3 of this paper, is produced by ionospheric reflection. During nighttime conditions, the sharper ionospheric gradients yield very distinct pulses that are clearly ionospheric reflections. In contrast, during daylight hours, ionospheric reflection pulses are much less distinct, and it is helpful to show unambiguously that these pulses are ionospheric in origin and can be used in estimation of an effective ionospheric reflection height.

[56] The waveforms presented here were computed with a finite difference time domain (FDTD) model of VLF propagation in the Earth-ionosphere waveguide [Hu and Cummer, 2006]. Curved ground geometry and arbitrary vertical inhomogeneity in the electron density profile are included. As we are interested in daytime conditions, we assumed an exponential electron density profile with $h' = 73$ km and $\beta = 0.40 \text{ km}^{-1}$, which are parameters that give a good statistical match to daytime sferics [Han and Cummer, 2010; Han et al., 2011] (see the first reference for the functional form).

[57] Figure A1 shows simulated vertical electric field waveforms for a 5-km long vertical lightning channel and a simple source current waveform (Gaussian pulse with a peak of 20 kA and a total charge moment change of 5.3 C km) at distances ranging from 100 to 400 km. Note that azimuthal magnetic field waveforms are almost identical for these ranges and frequencies. The waveforms have been aligned to

Table A1. Comparison of Time Differences From the Simulated Waveforms Shown in Figure A1 With the Expected Simple Time-of-Flight Differences

Distance (km)	Peak-to-Peak (μs)	Zero-to-Zero (μs)	Time of Flight (μs)
100	246	180	258
140	210	180	210
200	172	168	162
300	142	148	117
400	120	134	93

their peak values. The first pulse (initial half-cycle) shows a consistent shape, with diminishing amplitude with distance as expected. The second pulse (second positive half-cycle), although it is not well-defined, moves closer in time to the first pulse as the propagation distance increases. This is expected for an ionospheric reflection and suggests that this is its origin.

[58] Table A1 quantitatively compares pulse time differences from the simulated waveforms (both peak to peak and leading zero to leading zero) to the simple time-of-flight time differences (differences in arrival time of ground and first sky waves) computed geometrically for a curved Earth and an effective ionospheric reflection altitude of 73 km. The simple time-of-flight predictions are in closest agreement with the peak-to-peak time difference from the simulated waveforms, although the peak-to-peak delay becomes longer (relative to the time of flight) as propagation distance increases (consistent with a higher effective reflection altitude).

[59] These modest discrepancies are not surprising given the strong filtering that occurs in ionospheric reflection from a daytime ionosphere. Such frequency and distance dependent filtering makes it difficult to identify a precise “time” of the ionospheric reflection. However, both peak-to-peak and zero-to-zero time differences are in general agreement with simple time-of-flight predictions and further indicate that the origin of the second positive half-cycle is from ionospheric reflection.

[60] **Acknowledgments.** This research was supported in part by the University Scholars Program at the University of Florida, the NSF grants ATM-0852869, ATM-1047588, and ATM-1042198, and the DARPA NIMBUS program. The authors wish to thank Vaisala for providing NLDN data and the World Wide Lightning Location Network for providing locations for selected lightning strokes. The authors would also like to thank Dimitris Tsalikis and Amitabh Nag for their help with acquisition and processing of the data. Vijaya Bhaskar Somu helped with calculations of ionospheric reflection heights. Comments by Marcos Rubinstein, John Cramer, and Ken Cummins are appreciated.

References

Baba, Y., and V. A. Rakov (2007), Electromagnetic fields at the top of a tall building associated with nearby lightning return strokes, *IEEE Trans. Electromagn. Compat.*, *49*(3), 632–643.

Cheng, Z., and S. A. Cummer (2005), Broadband VLF measurements of lightning-induced ionospheric perturbations, *Geophys. Res. Lett.*, *32*, L08804, doi:10.1029/2004GL022187.

Cheng, Z., S. A. Cummer, H.-T. Su, and R.-R. Hsu (2007), Broadband very low frequency measurement of D region ionospheric perturbations caused by lightning electromagnetic pulses, *J. Geophys. Res.*, *112*, A06318, doi:10.1029/2006JA011840.

Cooray, V., and S. Lundquist (1982), On the characteristics of some radiation fields from lightning and their possible origin in positive ground flashes, *J. Geophys. Res.*, *87*, 11,203–11,214, doi:10.1029/JC087iC13p11203.

Cooray, V., and S. Lundquist (1985), Characteristics of the radiation fields from lightning in Sri Lanka in the tropics, *J. Geophys. Res.*, *90*, 6099–6109, doi:10.1029/JD090iD04p06099.

Cooray, V., V. A. Rakov, F. Rachidi, R. Montano, and C. A. Nucci (2008), On the relationship between the signature of close electric field and the equivalent corona current in lightning return stroke models, *IEEE Trans. Electromagn. Compat.*, *50*(4), 921–927.

Cummins, K. L. (2000), Continental-scale detection of cloud-to-ground lightning, *Trans. IEE Jpn.*, *120-B*(1), 2–5.

Cummins, K. L., and M. J. Murphy (2009), An overview of lightning locating systems: History, techniques, and data uses, with an in-depth look at the U.S. NLDN, *IEEE Trans. Electromagn. Compat.*, *51*(3), 499–518, doi:10.1109/TEMC.2009.2023450.

Cummins, K. L., A. E. Pifer, N. Honma, M. Pezze, T. Rogers, and M. Tatsumi (2010), Improved detection of winter lightning in the Tohoku region of Japan using Vaisala’s LS700X technology, paper presented at GROUND’2010 and 4th LPE, Braz. Soc. for Electr. Prot., Salvador, Brazil.

Cummins, K. L., N. Honma, A. E. Pifer, and M. Tatsumi (2011), Improved detection of winter lightning in the Tohoku region of Japan using Vaisala’s LS700x technology, paper presented at 3rd International Symposium on Winter Lightning, IEEE, Sapporo, Japan.

Han, F., and S. A. Cummer (2010), Midlatitude daytime D region ionosphere variability measured from radio atmospherics, *J. Geophys. Res.*, *115*, A10314, doi:10.1029/2010JA015715.

Han, F., S. A. Cummer, J. Li, and G. Lu (2011), Daytime ionospheric D region sharpness derived from VLF radio atmospherics, *J. Geophys. Res.*, *116*, A05314, doi:10.1029/2010JA016299.

Honma, N. (2010), Detection efficiency of the Tohoku IMPACT sensor network in winter, paper presented at 21st International Lightning Detection Conference, Vaisala, Orlando, Fla.

Hu, W., and S. A. Cummer (2006), An FDTD model for low and high altitude lightning-generated EM fields, *IEEE Trans. Antennas Propag.*, *54*, 1513–1522, doi:10.1109/TAP.2006.874336.

Hutchins, M. L., R. H. Holzworth, C. J. Rodger, and J. B. Brundell (2012), Far field power of lightning strokes as measured by the World Wide Lightning Location Network, *J. Atmos. Oceanic Technol.*, doi:10.1175/JTECH-D-11-00174.1, in press.

Inan, U. S., T. F. Bell, and J. V. Rodriguez (1991), Heating and ionization of the lower ionosphere by lightning, *Geophys. Res. Lett.*, *18*, 705–708, doi:10.1029/91GL00364.

Inan, U. S., S. A. Cummer, and R. A. Marshall (2010), A survey of ELF and VLF research on lightning-ionosphere interactions and causative discharges, *J. Geophys. Res.*, *115*, A00E36, doi:10.1029/2009JA014775.

Jerauld, J., V. A. Rakov, M. A. Uman, K. J. Rambo, D. M. Jordan, K. L. Cummins, and J. A. Cramer (2005), An evaluation of the performance characteristics of the U.S. National Lightning Detection Network in Florida using triggered lightning, *J. Geophys. Res.*, *110*, D19106, doi:10.1029/2005JD005924.

Kumar, S., A. Kumar, and C. J. Rodger (2008), Subionospheric early VLF perturbations observed at Suva: VLF detection of red sprites in the day?, *J. Geophys. Res.*, *113*, A03311, doi:10.1029/2007JA012734.

Laby, T. H., J. J. McNeill, F. G. Nicholls, and A. F. B. Nickson (1940), Waveform, energy and reflexion by the ionosphere, of atmospherics, *Proc. R. Soc. A*, *174*, 145–163.

Lin, Y. T., M. A. Uman, J. A. Tiller, R. D. Brantley, W. H. Beasley, E. P. Krider, and C. D. Weidman (1979), Characterization of lightning return stroke electric and magnetic fields from simultaneous two station measurements, *J. Geophys. Res.*, *84*, 6307–6314, doi:10.1029/JC084iC10p06307.

Mallick, S., V. A. Rakov, D. Tsalikis, A. Nag, C. Biagi, D. Hill, D. M. Jordan, M. A. Uman, and J. A. Cramer (2011), On remote measurements of lightning peak currents, paper presented at XIV International Conference on Atmospheric Electricity, ICAE, Rio de Janeiro, Brazil.

Marshall, R. A., U. S. Inan, and V. S. Glukhov (2010), Elves and associated electron density changes due to cloud-to-ground and in-cloud lightning discharges, *J. Geophys. Res.*, *115*, A00E17, doi:10.1029/2009JA014469.

Master, M. J., M. A. Uman, W. H. Beasley, and M. Darveniza (1984), Lightning induced voltages on power lines: Experiment, *IEEE Trans. Power Appar. Syst.*, *103*, 2519–2529.

Nag, A. (2010), Characterization and modeling of lightning processes with emphasis on compact intracloud discharges, PhD dissertation, Univ. of Fla., Gainesville.

Nag, A., et al. (2011a), Evaluation of NLDN performance characteristics using rocket-triggered lightning data acquired in 2004–2009, *J. Geophys. Res.*, *116*, D02123, doi:10.1029/2010JD014929.

Nag, A., V. A. Rakov, and J. A. Cramer (2011b), Remote measurements of currents in cloud lightning discharges, *IEEE Trans. Electromagn. Compat.*, *53*(2), 407–413.

- Pavlick, A., D. E. Crawford, and V. A. Rakov (2002), Characteristics of distant lightning electric fields, paper presented at International Conference on Probabilistic Methods Applied to Power Systems, Univ. of Cassino, Naples, Italy.
- Rakov, V. A., and W. G. Tuni (2003), Lightning electric field intensity at high altitudes: Inferences for production of elves, *J. Geophys. Res.*, *108*(D20), 4639, doi:10.1029/2003JD003618.
- Rakov, V. A., and M. A. Uman (1998), Review and evaluation of lightning return stroke models including some aspects of their application, *IEEE Trans. Electromagn. Compat.*, *40*, 403–426, doi:10.1109/15.736202.
- Rakov, V. A., and M. A. Uman (2003), *Lightning: Physics and Effects*, 687 pp., Cambridge Univ. Press, Cambridge, U. K.
- Rakov, V. A., R. Thottappillil, and M. A. Uman (1992), On the empirical formula of Willett et al. relating lightning return stroke peak current and peak electric field, *J. Geophys. Res.*, *97*, 11,527–11,533, doi:10.1029/92JD00720.
- Rodger, C. J., S. Werner, J. B. Brundell, E. H. Lay, N. R. Thomson, R. H. Holzworth, and R. L. Dowden (2006), Detection efficiency of the VLF World-Wide Lightning Location Network (WWLLN): Initial case study, *Ann. Geophys.*, *24*, 3197–3214, doi:10.5194/angeo-24-3197-2006.
- Rowland, H. L., R. F. Fernsler, and P. A. Bernhardt (1996), Breakdown of the neutral atmosphere in the D region due to lightning driven electromagnetic pulses, *J. Geophys. Res.*, *101*, 7935–7945, doi:10.1029/95JA03519.
- Serhan, G. I., M. A. Uman, D. G. Childers, and Y. T. Lin (1980), The RF spectra of first and subsequent lightning return strokes in the 1–200 km range, *Radio Sci.*, *15*, 1089–1094, doi:10.1029/RS015i006p01089.
- Shoory, A., F. Rachidi, M. Rubinstein, R. Moini, and S. H. H. Sadeghi (2009), Why do some lightning return stroke models not reproduce the far-field zero crossing?, *J. Geophys. Res.*, *114*, D16204, doi:10.1029/2008JD011547.
- Smith, D. A., M. J. Heavner, A. R. Jacobson, X. M. Shao, R. S. Massey, R. J. Sheldon, and K. C. Wiens (2004), A method for determining intracloud lightning and ionospheric heights from VLF/LF electric field records, *Radio Sci.*, *39*, RS1010, doi:10.1029/2002RS002790.
- Taranenko, Y. N., U. S. Inan, and T. F. Bell (1993), The interaction with the lower ionosphere of electromagnetic pulses from lightning: Excitation of optical emissions, *Geophys. Res. Lett.*, *20*, 2675–2678, doi:10.1029/93GL02838.
- Taylor, W. L. (1963), Radiation field characteristics of lightning discharges in the band 1 kc/s to 100 kc/s, *J. Res. Natl. Bur. Standards D*, *67*, 539–550.
- Thottappillil, R., M. A. Uman, and G. Diendorfer (1991), Influence of channel base current and varying return stroke speed on the calculated fields of three important return stroke models, paper presented at 1991 International Conference on Lightning and Static Electricity, NASA, Cocoa Beach, Fla.
- Willett, J. C., J. C. Bailey, V. P. Idone, A. Eybert-Berard, and L. Barret (1989), Submicrosecond intercomparison of radiation fields and currents in triggered lightning return strokes based on the transmission-line model, *J. Geophys. Res.*, *94*, 13,275–13,286, doi:10.1029/JD094iD11p13275.